

Superimposed Oscillations in Brane Inflation

Santiago Ávila^{*a,c}, Jérôme Martin^{†b}, Danièle A. Steer^{‡c,b}

^a *Departamento de Física Teórica, Facultad de Ciencias,*

Universidad Autónoma de Madrid, 28049 Cantoblanco, Madrid, Spain

^b *Institut Astrophysique de Paris, UMR 7095-CNRS,*

Université Pierre et Marie Curie, 98bis Boulevard Arago, 75014 Paris, France

^c *APC, Université Paris-Diderot, CNRS/IN2P3, CEA/IRFU and Observatoire de Paris,
10 rue Alice Domon et Léonie Duquet, 75205 Paris Cedex 13, France*

(Dated: April 12, 2013)

In canonical scalar field inflation, the Starobinsky model (with a linear potential but discontinuous slope) is remarkable in that though slow-roll is violated, both the power-spectrum and bi-spectrum can be calculated exactly analytically. The two-point function is characterised by different power on large and small scales, and a burst of small amplitude superimposed oscillations in between. Motivated by string-theory models with stuck branes, we extend this analysis to Dirac Born Infeld (DBI) inflation, for which generalised slow-roll is violated at the discontinuity and a rapid variation in the speed of sound c_s occurs. In an attempt to characterise the effect of non-linear kinetic terms on the oscillatory features of the primordial power-spectrum, we show that the resulting power spectrum has a shape and features which differ significantly from those of the standard Starobinsky model. In particular, the power-spectrum now takes very similar scale invariant values on large and small scales, while on intermediate scales it is characterised by much larger amplitude and higher frequency superimposed oscillations. We also show that calculating non-Gaussianities in this model is a complicated but interesting task since all terms in the cubic action now contribute. Investigating whether the superimposed oscillations could fit to the Planck Cosmic Microwave Background (CMB) data (for instance by explaining the large scale Planck anomalies) with, at the same time, small non-Gaussianities remains an intriguing and open possibility.

I. INTRODUCTION

It is by now a near certainty that the universe underwent a period of accelerated expansion — inflation — early in its history. Indeed, the spectacular Planck data [1, 2] is entirely compatible with Standard Single Field Inflation (SSFI) in the slow-roll regime, and with a canonical kinetic term [3]. However, the nature of the inflaton field still remains a mystery, and on the theoretical side much work has been carried out in the last years with the aim of trying to embed the inflationary scenario in a high-energy theory such as string theory. This paper fits into such a “top-down” approach. In particular our focus is on string motivated models (see below) in which, because generalised slow-roll is violated for a few e-folds, oscillations are generated in the power spectrum. Our aim is to determine precisely the observational predictions of this class of models. In the process we will characterise how, for a given inflaton potential, the properties of the superimposed oscillations in $\mathcal{P}_\zeta(k)$ — amplitude and frequency for example — depend on non-standard kinetic terms in the Lagrangian for the inflaton.

The model we study is closely related to the so-called Starobinsky model [4, 5] for which the potential $V(\phi)$ is linear with a sharp change of slope at a certain ϕ_0 :

$$V(\phi) = \begin{cases} V_0 + A_+ (\phi - \phi_0) & \text{for } \phi > \phi_0, \\ V_0 + A_- (\phi - \phi_0) & \text{for } \phi < \phi_0. \end{cases} \quad (1)$$

In the following we will take $A_+ > A_-$. The change in slope causes a short, of order one in e -folds, period of fast roll, and remarkably (in SSFI with standard kinetic terms) both the power spectrum and bispectrum can be determined exactly analytically (in all range of parameter space). To our knowledge, this is the only model in SSFI for which any exact statements can be made. One finds [4] that there is a sharp rise in the power-spectrum $\mathcal{P}_\zeta(k)$ on scales $k \sim k_0$ (where k_0 is the mode that left the Hubble radius at $\phi = \phi_0$), with

$$\lim_{k/k_0 \rightarrow 0} \mathcal{P}_\zeta^{\text{CS}}(k) = \left(\frac{H_0}{2\pi}\right)^2 \left(\frac{3H_0^2}{A_+}\right)^2, \quad \lim_{k/k_0 \rightarrow \infty} \mathcal{P}_\zeta^{\text{CS}}(k) = \left(\frac{H_0}{2\pi}\right)^2 \left(\frac{3H_0^2}{A_-}\right)^2, \quad (2)$$

* E-mail: santiago.avila@uam.es

† E-mail: jmartin@iap.fr

‡ E-mail: steer@apc.univ-paris7.fr

where H_0 is the Hubble scale at the time when $\phi = \phi_0$, and CS denotes the ‘canonical’ Starobinsky model. Thus the increase in power is proportional to $A_-^{-2} - A_+^{-2}$, and it is followed by small oscillations for $k \gtrsim k_0$ whose amplitude are rapidly damped out. The different contributions to the bi-spectrum can also be calculated analytically [6, 7] in terms of A_\pm and the third parameter of the model H_0 , and some ranges of parameter space are ruled out by recent constraints on f_{NL} from Cosmic Microwave Background (CMB) data [2, 8].

Here, motivated by string-theory, we focus on Dirac Born Infeld (DBI) brane inflation (see *e.g.* [9–14]) with action

$$S = - \int d^4x \sqrt{-g} \left[M_{\text{Pl}}^2 R + T(\phi) \sqrt{1 + \frac{1}{T(\phi)} g^{\mu\nu} \partial_\mu \phi \partial_\nu \phi} + V(\phi) - T(\phi) \right], \quad (3)$$

where R is the Ricci scalar and M_{Pl} the reduced Planck mass. As usual $T(\phi)$, which we call the ‘brane tension’ from the physical origin of action (3), is determined by the warp factor of the 10 dimensional metric in which the brane moves. Provided it is continuous, its precise form is essentially unimportant for this analysis, though to be concrete we take

$$T(\phi) = \frac{\phi^4}{\lambda} \quad (4)$$

which is typical for anti de Sitter warp factors. The potential $V(\phi)$ has contributions coming from the interaction between the brane and the background, as well as any other branes which may be present in the geometry. Its exact expression is not known and here, without attempting to concretely realise the embedding of this model within string-theory, we suppose it is given by (1). Such a sudden jump at ϕ_0 can be thought of as mimicking the presence of a trapped brane stuck at a fixed point of an orbifold symmetry [15], and potentials of this kind have been studied in the DBI-literature before *e.g.* [16]. In particular, if one considers the excitation of particles living on the trapped brane, then these can backreact on the inflaton dynamics [17], though the effect has been shown to be small. Note that in the limit in which the sound speed $c_s \rightarrow 1$, our model reduces to the standard Starobinsky-model discussed above. Our model may not be completely realistic from a string theory point of view but its crucial advantage is that it allows us to derive explicit analytical results, which can be compared to known results for the standard Starobinsky model. We believe that the scenario studied here represents the best compromise between cases in which the string model building problem can be properly addressed (often at the expense of solving the equations numerically), and over simplified situations in which analytical results can be easily derived.

Just as in the standard Starobinsky model, in the DBI case, generalised slow-roll is broken for order one e-folds around ϕ_0 . Thus c_s also changes rapidly, and we expect oscillations to be generated in the power-spectrum. How does the shape of $\mathcal{P}_\zeta(k)$ depend on the non-standard kinetic terms? Are the amplitude and wavelength of the oscillations sensitive to the non-linear structure of the Lagrangian? In this paper not only do we determine $\mathcal{P}_\zeta(k)$ numerically for all c_s , but we also show that the model is essentially completely soluble analytically in the $c_s \ll 1$ limit, in terms of the parameters of the potential A_\pm . Due to the non-linear kinetic terms in the action, $\mathcal{P}_\zeta(k)$ differs significantly from that of the canonical SSFI Starobinsky model discussed above. Indeed, the action given in (3) now contains a second dimensionful potential $T(\phi)$ and it is this, rather than A_\pm , which determines the power-spectrum on small and large scales:

$$\begin{aligned} \lim_{k/k_0 \rightarrow 0} \mathcal{P}_\zeta(k) &= \left(\frac{H_0}{2\pi} \right)^2 \left(\frac{H_0^2}{T_0} \right) \left[\left(1 - \frac{A_-}{2A_+} \right) \left(1 + \frac{A_-}{A_+} \right)^2 \right], \\ \lim_{k/k_0 \rightarrow \infty} \mathcal{P}_\zeta(k) &= \left(\frac{H_0}{2\pi} \right)^2 \left(\frac{H_0^2}{T_0} \right), \end{aligned}$$

where $T_0 = T(\phi_0)$. As opposed to the canonical Starobinsky model in which there is a sharp rise in power across k_0 if $A_- \ll A_+$, in the DBI-Starobinsky model there is *no* rise in power in this case. Rapid variations of c_s occur when the field crosses ϕ_0 , and these give rise to large amplitude, high frequency, superimposed oscillations in $\mathcal{P}_\zeta(k)$ which we will discuss in section III. An interesting question is whether or not these oscillations could fit the Planck data, for instance explaining the large scale Planck anomalies, while also remaining compatible with constraints on non-Gaussianities. Indeed, as we discuss in the conclusions, an interesting new feature of this model is that we expect non-Gaussianities to be sourced predominantly from two (or more) coupled vertices, leading to a complicated structure. While it might be expected that the constraints are strong at least for $c_s \ll 1$, for larger c_s the situation regarding non-Gaussianities is much less clear while the large amplitude superimposed oscillations remain in the power-spectrum.

In the context of SSFI, the development of models leading to oscillations was motivated by observed features in the power-spectrum of CMB temperature fluctuations [18–22]. Indeed, they may find their origin in initial conditions, arising for instance from non-Bunch-Davies initial conditions (see *e.g.* [19, 23]), or from deviations from slow-roll in

SSFI. Amongst the models studied in the literature are, for instance, potentials whose derivative is discontinuous [4, 6], as well as potentials which contain a step (*e.g.* [5, 24]), or a sinusoidal modulation (*e.g.* [25–27]). Though these features can fit data better than a nearly scale invariant power-spectrum (see for example [1, 28]), this is at the expense of including extra parameters into the potential meaning that the statistical significance of the features is not so obvious [29]. Other than solving for the power-spectrum numerically [30–32], some semi-analytical methods have been developed [33, 34] though these are generally valid only in certain limiting cases, for example if the step is small or if the scalar field and metric perturbations decouple [27].

In models with non-standard kinetic terms, the consequences of rapid variations in c_s in k -inflation have been investigated (both for the power-spectrum and bispectrum) using the effective field theory formalism in [35]. The “generalised slow-roll approximation” has been extended to k -inflation [36], and applied to DBI-inflation in [37], though there the authors considered a step-like feature in $T(\phi)$. Notice that Ref. [38] also carries out a detailed analysis of the signatures of step-like feature in both $T(\phi)$ and $V(\phi)$.

The structure of this paper is the following. In section II we first discuss the background evolution of the system and define the generalised slow-roll parameters (subsection II A). At this point, our discussion is for a general potential $V(\phi)$. In subsection II B we focus on the Starobinsky model itself, with potentials $V(\phi)$ and $T(\phi)$ given in Eqs. (1) and (4) respectively. From the form of $V(\phi)$ we are able to derive exact results regarding the behaviour of the system at the transition $\phi = \phi_0$, and these enable us to determine the evolution of all the slow-roll parameters analytically, even when slow-roll is violated. Our results, valid in the DBI limit $c_s \ll 1$, are shown to match perfectly with a full numerical solution of the background equations. In section III, using these exact results, we show that the calculation the power-spectrum $\mathcal{P}_\zeta(k)$ reduces to solving single differential equation with particular time-dependent coefficients that we specify. The resulting power-spectrum is shown to be in perfect agreement with a full numerical determination of the same quantity. We also determine analytically the dependence of $\mathcal{P}_\zeta(k)$ on A_\pm , on large and small scales. Finally we summarise our main results in the section IV, where we discuss in detail the different shape of the canonical and DBI Starobinsky power-spectra. We also present a few considerations on the calculation of non-Gaussianities in this model and mention interesting directions for future work.

II. BACKGROUND EQUATIONS AND SLOWLY VARYING PARAMETERS

A. Exact Equations

For arbitrary potentials $V(\phi)$ and $T(\phi)$, and working in a spatially flat Friedmann-Lemaître-Robertson-Walker (FLRW) background geometry with metric $ds^2 = -dt^2 + a^2(t)d\mathbf{x}^2$, the Friedmann and scalar field equations of motion following from Eq. (3) are given, respectively, by

$$H^2 = \frac{1}{3M_{\text{Pl}}^2} [(\gamma - 1)T + V], \quad (5)$$

$$\ddot{\phi} + \frac{3H}{\gamma^2} \dot{\phi} + \frac{3\gamma - \gamma^3 - 2}{2\gamma^3} T_\phi + \frac{1}{\gamma^3} V_\phi = 0. \quad (6)$$

Here a dot/subscript ϕ denotes derivative with respect to cosmic time t /field ϕ respectively, and $H = \dot{a}/a$ is the Hubble parameter. The Lorentz factor γ is related to the square-root in (3) and is inversely proportional to the sound-speed c_s

$$\gamma(\dot{\phi}, \phi) \equiv \frac{1}{c_s} = \frac{1}{\sqrt{1 - \dot{\phi}^2/T(\phi)}}. \quad (7)$$

Later on we will mainly consider $c_s \ll 1$, which is the opposite limit to the standard inflationary case, obtained when $c_s \rightarrow 1$ (or $\gamma \rightarrow 1$). For the moment, however, we leave γ arbitrary and all the expressions in this section are exact.

In general, due to their complexity, Eqs. (5) and (6) cannot be integrated exactly unless numerical methods are used. However, it is also interesting to have analytical approximations and for this reason, we now define the horizon-flow parameters. While in standard inflation they are defined as the successive derivatives of the Hubble parameter [39–41], in DBI-inflation a second hierarchy of parameters must be introduced in order to describe the evolution of the sound speed (or equivalently γ). This hierarchy is defined as the successive derivatives of the Lorentz factor with respect to the number of e-folds $N = \ln(a/a_{\text{in}})$ (where a_{in} is the initial value of the scale factor), see *e.g.* [42]. Thus

the slow-roll (or slowly-varying) parameters of DBI-inflation are given by

$$\epsilon_{n+1} = \frac{d \ln |\epsilon_n|}{dN}, \quad \epsilon_0 \equiv \frac{H_{\text{in}}}{H}, \quad (8)$$

$$\delta_{n+1} = \frac{d \ln |\delta_n|}{dN}, \quad \delta_0 \equiv \frac{c_{\text{sin}}}{c_s} = \frac{\gamma}{\gamma_{\text{in}}}. \quad (9)$$

The slow-roll approximation will consist in taking $|\epsilon_i| \ll 1$ and $|\delta_i| \ll 1$ and in sections [IIB](#) we will see that this greatly simplifies the equations describing the evolution of the system.

For the moment, however, we make no approximation. In order to write down the exact expressions for the first few slow-roll parameters, it is useful to note from [\(5\)](#) and [\(6\)](#) that the time derivative of the Hubble parameter is given by

$$\dot{H} = -\gamma \frac{\dot{\phi}^2}{2M_{\text{Pl}}^2}, \quad (10)$$

so that $H_\phi^2 = T(\phi)(\gamma^2 - 1)/(4M_{\text{Pl}}^4)$. From here we can extract a very useful expression for γ , namely

$$\gamma = \sqrt{1 + 4M_{\text{Pl}}^4 \frac{H_\phi^2}{T}} \quad (11)$$

which will be used extensively below, and in terms of which derivatives of N can easily be calculated

$$\frac{dN}{d\phi} = -\frac{\gamma}{2M_{\text{Pl}}^2} \frac{H}{H_\phi} = -\frac{1}{2M_{\text{Pl}}^2} \frac{H}{H_\phi} \sqrt{1 + 4M_{\text{Pl}}^4 \frac{H_\phi^2}{T}}. \quad (12)$$

The exact expressions for the first flow parameters are then

$$\epsilon_1 = \frac{2M_{\text{Pl}}^2}{\gamma} \left(\frac{H_\phi}{H} \right)^2 = \frac{T(\gamma^2 - 1)}{2M_{\text{Pl}}^2 \gamma H^2}, \quad (13)$$

$$\epsilon_2 = -\frac{4M_{\text{Pl}}^2 H_{\phi\phi}}{H\gamma} + 2\epsilon_1 - \delta_1, \quad (14)$$

$$\delta_1 = -\frac{2M_{\text{Pl}}^2}{\gamma^2} \frac{H_\phi}{H} \frac{d\gamma}{d\phi} = -\frac{2M_{\text{Pl}}^2}{\gamma^2} \frac{H_\phi}{HT} [6M_{\text{Pl}}^2 H H_\phi - V_\phi - (\gamma - 1) T_\phi], \quad (15)$$

$$\delta_1 \delta_2 = \frac{3}{2} \left(\frac{\gamma^2 - 1}{\gamma^2} \right) (4\epsilon_1 - \epsilon_2 - \delta_1) - \frac{3}{2} \epsilon_2 \delta_1 + 4\epsilon_1 \delta_1 + \frac{(\gamma^2 + 7)}{(\gamma^2 - 1)} \frac{\delta_1^2}{2} - \frac{(\gamma^2 - 1)}{\gamma^3 H^2} [V_{\phi\phi} + (\gamma - 1) T_{\phi\phi}], \quad (16)$$

$$\begin{aligned} \epsilon_2 \epsilon_3 + \delta_1 \delta_2 &= -3(\epsilon_2 - 4\epsilon_1 + \delta_1) + 2\epsilon_1 \epsilon_2 + 2\delta_1^2 \left(\frac{\gamma^2}{\gamma^2 - 1} \right) - \frac{1}{2} (\epsilon_2 - 2\epsilon_1 + \delta_1) (\epsilon_2 - 4\epsilon_1 + 3\delta_1) \\ &\quad - \frac{1}{\gamma H^2} \left[2V_{\phi\phi} + \frac{T_{\phi\phi}}{\gamma} (\gamma - 1)^2 \right]. \end{aligned} \quad (17)$$

One can also proceed the other way round, and express some important background quantities in terms of the slow-roll parameters. For instance, on rewriting T in terms of ϵ_1 using [\(13\)](#), the Friedmann equation [\(5\)](#) can be re-expressed as

$$H^2 = \frac{V(\phi)}{3M_{\text{Pl}}^2} \left[1 - \frac{2\gamma}{3(\gamma + 1)} \epsilon_1 \right]^{-1}. \quad (18)$$

As we will see in the next sub-section, this equation turns out to be crucial in order to understand the behaviour of the system. On differentiating with respect to ϕ and using the definition of the slow-roll parameters yields

$$M_{\text{Pl}} \frac{V_\phi}{V} = +\sqrt{2\gamma\epsilon_1} \left[1 + \frac{1}{3 - 2\gamma\epsilon_1/(\gamma + 1)} \frac{\gamma}{\gamma + 1} \left(\epsilon_2 + \frac{\delta_1}{\gamma + 1} \right) \right]. \quad (19)$$

A further derivative would give $V_{\phi\phi}$, but the result is somewhat tedious, so we only give it below to leading order in slow-roll parameters. Finally, one can also derive a useful relation for the derivative of the brane tension, namely

$$M_{\text{Pl}} \frac{T_\phi}{T} = +\sqrt{\frac{\gamma}{2\epsilon_1}} \left[2\epsilon_1 + \left(\frac{\gamma^2 + 1}{\gamma^2 - 1} \right) \delta_1 - \epsilon_2 \right]. \quad (20)$$

As already mentioned, the above equations are all exact and valid for any potential and any brane tension. In the next subsection, we focus on the Starobinsky model itself.

B. Application to the Starobinsky Model

We now consider the DBI-Starobinsky model, with potentials $V(\phi)$ and $T(\phi)$ given in Eqs. (1) and (4). In this case, Eqs. (5) and (6) still cannot be integrated analytically. Nevertheless, as we now show, some exact results about the behaviour of the system at the transition can be established.

1. Exact Results for Starobinsky Potential

Suppose that the field is rolling down the potential (1), starting at a value ϕ_{in} with $\phi_{\text{in}} > \phi_0$. Since V_ϕ is discontinuous at $\phi = \phi_0$ it follows from Eq. (6) that both ϕ and $\dot{\phi}$ (and thus γ) are continuous, but $\ddot{\phi}$ is discontinuous. Thus $\dot{\gamma}$ is also discontinuous, and its jump can be read off from the following exact equation [consequence of Eqs. (5) and (6)]

$$\dot{\gamma} = -\frac{\dot{\phi}}{T} \left[3H\gamma\dot{\phi} + V_\phi + (\gamma - 1)T_\phi \right], \quad (21)$$

which leads to

$$[\dot{\gamma}]_\pm = -\frac{\dot{\phi}}{T} [V_\phi]_\pm = \Delta A \frac{\dot{\phi}}{T}, \quad (22)$$

where $\Delta A \equiv A_- - A_+ < 0$. This can be rewritten in terms of derivatives with respect to N as

$$\left[\frac{d\gamma}{dN} \right]_\pm = -\frac{\gamma^2 - 1}{M_{\text{Pl}} H^2 \gamma} \frac{\Delta A}{\sqrt{2\epsilon_1 \gamma}}. \quad (23)$$

We now study the behaviour of the slow-roll parameters at the transition. From Eq. (13), it follows that ϵ_1 remains continuous. However, since ϵ_2 is defined in terms of derivatives of ϵ_1 which itself contains γ [see Eq. (13)], the second horizon flow parameter ϵ_2 is discontinuous. (This is also true in the SSFI-Starobinsky model.) Moreover, following from the definition in terms of γ , the parameter δ_1 is also discontinuous. Its jump across the discontinuity is related to that of ϵ_2 from Eq. (20):

$$[\delta_1]_\pm \left(\frac{\gamma^2 + 1}{\gamma^2 - 1} \right) \Big|_{\phi_0} = [\epsilon_2]_\pm. \quad (24)$$

If initial conditions at the beginning of inflation are such that all slow-roll parameters are small, it therefore follows that the DBI-Starobinsky model is characterised by a continuous ϵ_1 which remains small all the time (hence, inflation never comes to an end), and by parameters ϵ_2 and δ_1 which are small far from the transition, but jump and can be large at the discontinuity. In this sense, the DBI-Starobinsky model is a direct generalisation of the canonical Starobinsky model for which $\epsilon_1 \ll 1$ and ϵ_2 jumps at the transition. The new ingredient is, of course, the presence of the parameter δ_1 and we have just seen that this parameter has a jump comparable to that of ϵ_2 , in particular when $\gamma \gg 1$, see Eq. (24).

2. Integration of Equations of Motion: Numerics and Analytic Approximation

Having understood the broad behaviour of the background quantities (without using any approximation), we now aim to understand their evolution in a more detailed fashion, at the quantitative level. As already mentioned, since Eqs. (5) and (6) cannot be integrated exactly analytically, we have to rely either on numerical calculations or on approximations. In the following, we use both.

Let us start with the field ϕ . In Fig. 1, we show the exact evolution of the field (we have numerically integrated the exact equations of motion) for two sets of parameters and initial conditions. In order to understand this behaviour, first notice from Eq. (18) that in the slow-roll regime when $\epsilon_1 \ll 1$, and for all γ , the Friedmann equation (18) reduces to

$$H^2 \simeq \frac{1}{3M_{\text{Pl}}^2} V(\phi). \quad (25)$$

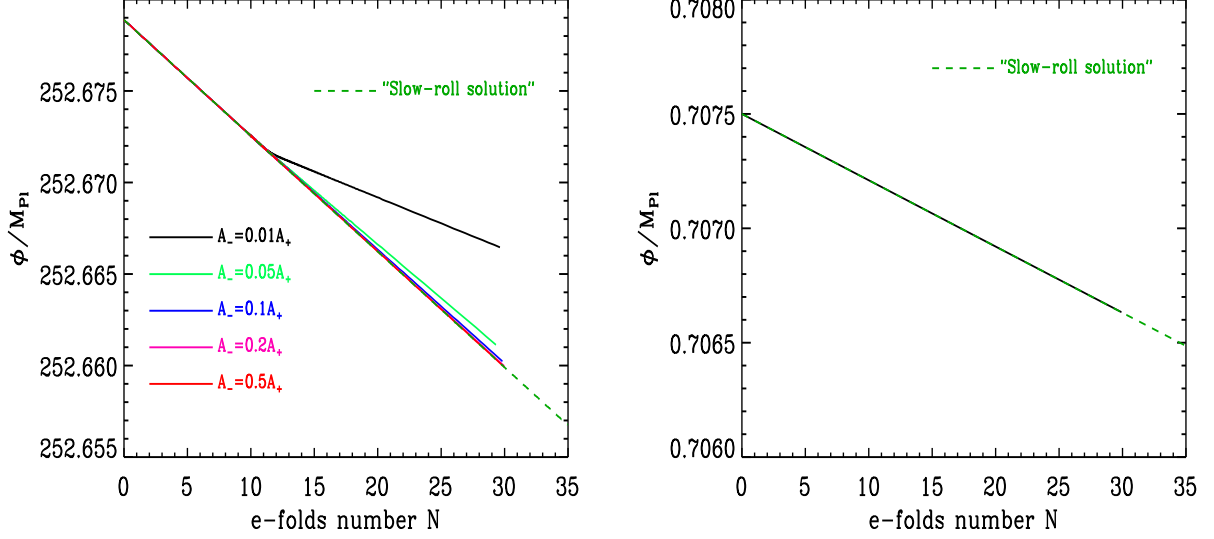


FIG. 1: **Left panel:** Evolution of the field ϕ for the choice $\epsilon_{1\text{in}} \simeq 10^{-5}$, $\epsilon_{2\text{in}} \simeq 2.5 \times 10^{-5}$, $\delta_{1\text{in}} \simeq 1.5 \times 10^{-5}$, $\gamma_{\text{in}} \simeq 50$, $\phi_{\text{in}}/M_{\text{Pl}} \simeq 252.6788$, $H_{\text{in}}/M_{\text{Pl}} \simeq 3.97 \times 10^{-8}$ and $N_0 = 10$, where N_0 is the number of e-folds at which the field goes through the transition. This implies $V_0/M_{\text{Pl}}^4 \simeq 4.71 \times 10^{-15}$, $\lambda \simeq 6.45 \times 10^{30}$, $\phi_0/M_{\text{Pl}} \simeq 252.6725$ and $A_+/M_{\text{Pl}}^3 \simeq 1.49 \times 10^{-16}$. In the following this set of parameters is named “run one”. The black solid curve corresponds to $A_- = 0.01A_+$, the solid green one to $A_- = 0.05A_+$, the solid blue one to $A_- = 0.1A_+$, the solid pink one to $A_- = 0.2A_+$ and, finally, the solid red one to $A_- = 0.5A_+$. The presence of the transition at $N_0 = 10$ is easily visible. We see that the greater the change in the slopes, the more the trajectory is modified after the transition. The dark green dashed line represents the slow-roll solution given by Eq. (29). The slow-roll trajectory is not affected by the transition because, in the approximation used there, this trajectory no longer depends on the parameters A_{\pm} . If the initial velocity is not very large and the slope change important, then the actual trajectory can significantly deviates from the slow-roll, see the example of the black solid curve. Otherwise, the agreement is excellent. **Right panel:** evolution of the scalar field for another set of parameters, namely $\epsilon_{1\text{in}} \simeq 7.25 \times 10^{-7}$, $\epsilon_{2\text{in}} \simeq -7.98 \times 10^{-5}$, $\delta_{1\text{in}} \simeq 8.27 \times 10^{-5}$, $\gamma_{\text{in}} \simeq 1723.33$, $\phi_{\text{in}}/M_{\text{Pl}} \simeq 0.7075$, $H_{\text{in}}/M_{\text{Pl}} \simeq 1.82 \times 10^{-9}$, $N_0 \simeq 17.24$. This implies that $V_0/M_{\text{Pl}}^4 \simeq 9.98 \times 10^{-18}$, $\lambda \simeq 8.95 \times 10^{25}$, $\phi_0/M_{\text{Pl}} \simeq 0.7070$, $A_+/M_{\text{Pl}}^3 \simeq 4.98 \times 10^{-19}$ and $A_- = 0.01A_+$. In the following, we denote this set of parameters by “run two”. The solid black line represents the exact trajectory while the dark green dashed line represents the slow-roll solution given by Eq. (29). Despite the fact that $A_- = 0.01A_+$, as for the solid black line in the left panel, the agreement between the numerical and slow-roll solutions, is now very good. This is due to the fact that, for run two, the Lorentz factor γ is larger. As a consequence, the field arrives at the transition with a higher velocity and, therefore, is less sensitive to the changes in the slopes.

It is remarkable that, despite its intrinsic complexity in DBI inflation, the Friedmann equation exactly reduces to its standard counterpart when $\epsilon_1 \ll 1$. Thus we also have

$$2M_{\text{Pl}} \frac{H_\phi}{H} \simeq M_{\text{Pl}} \frac{V_\phi}{V} \simeq +\sqrt{2\gamma\epsilon_1}. \quad (26)$$

Now, the dynamics of $\phi(N)$ can be obtained from the exact identity (12) which, for a slow-roll trajectory [using Eqs. (25) and (26)], reduces to

$$N(\phi) \simeq \pm \frac{1}{M_{\text{Pl}}^2} \int_{\phi_{\text{in}}}^{\phi} d\psi \sqrt{\left(\frac{V}{V_\psi}\right)^2 + M_{\text{Pl}}^2 \frac{V}{3T}}. \quad (27)$$

Notice that this expression is in fact valid for any potential and any brane tension provided the slow-roll approximation holds. It was established for the first time in Ref. [43].

For the DBI-Starobinsky model with potential given in (1), Eq. (27) yields

$$N(\phi) = -\frac{1}{M_{\text{Pl}}^2} \int_{\phi_{\text{in}}}^{\phi} d\psi \frac{V_0 + A_{\pm}(\psi - \phi_0)}{A_{\pm}} \sqrt{1 + M_{\text{Pl}}^2 \frac{\lambda A_{\pm}^2}{3\psi^4 [V_0 + A_{\pm}(\psi - \phi_0)]}},$$

where we have chosen the minus sign since for the Starobinsky potential N increases as the field rolls down the potential towards smaller ϕ . Notice that the origin of the square-root is the γ factor in (12). The above expression

is still too complicated to allow an exact integration to determine the field trajectory: further assumptions must be made, and the first we make is to assume vacuum domination $V_0 \gg A_\pm(\psi - \phi_0)$ for all ψ . Then the trajectory is given by

$$N(\phi) \simeq -\frac{1}{M_{\text{Pl}}^2} \frac{V_0}{A_\pm} \int_{\phi_{\text{in}}}^{\phi} d\psi \sqrt{1 + \frac{\lambda A_\pm^2}{3V_0 M_{\text{Pl}}^2} \left(\frac{M_{\text{Pl}}}{\psi}\right)^4} \quad (28)$$

which results in Elliptic functions. Since this is still not especially illuminating, we make a second assumption, namely that we work in the DBI regime $\gamma \gg 1$, or equivalently $c_s \ll 1$. Referring to (11) this implies that we neglect the “1” in γ , which in Eq. (28) translates into

$$N(\phi) \simeq -\int_{\phi_{\text{in}}}^{\phi} d\psi \frac{H}{\sqrt{T}} = -\frac{1}{M_{\text{Pl}}} \sqrt{\frac{V_0 \lambda}{3}} \int_{\phi_{\text{in}}}^{\phi} d\psi \frac{1}{\psi^2}.$$

The solution is

$$\frac{1}{\phi(N)} = \frac{1}{\phi_{\text{in}}} - M_{\text{Pl}} \sqrt{\frac{3}{\lambda V_0}} N = \frac{1}{\phi_0} - M_{\text{Pl}} \sqrt{\frac{3}{\lambda V_0}} (N - N_0), \quad (29)$$

where N_0 denotes the number of e-folds when ϕ reaches the transition at ϕ_0 . The shortcoming of this expression is that, because of our successive approximations — vacuum domination, slow-roll $\epsilon_1 \ll 1$, and DBI-regime $\gamma \gg 1$ — we have lost the dependence on the coefficients A_\pm . The exact evolution of the scalar field is compared to the slow-roll trajectory (29) in Fig. 1.

We now study Lorentz factor γ given in Eq. (11) in more detail. Its exact (numerically solved) evolution is shown in Fig. 2. If the slow-roll approximation is satisfied (that is to say far from the point where the derivative of the potential is discontinuous), then

$$\gamma_{\text{sr}}(\phi) \simeq \sqrt{1 + \frac{\lambda M_{\text{Pl}}^2 A_\pm^2}{3\phi^4 [V_0 + A_\pm(\phi - \phi_0)]}} \simeq \sqrt{1 + \frac{\lambda M_{\text{Pl}}^2 A_\pm^2}{3\phi^4 V_0}}, \quad (30)$$

where the last expression is valid in the vacuum dominated regime. Furthermore, in the DBI regime $\gamma \gg 1$, the second term in the square root must dominate so that

$$\gamma_{\text{sr}}^{(\pm)}(N) \simeq \sqrt{\frac{\lambda}{3V_0}} \frac{M_{\text{Pl}} A_\pm}{\phi^2(N)}, \quad (31)$$

where $\phi(N)$ is given in (29). Notice that the Lorentz factor does depend on A_\pm .

During the transition, the above expression is clearly no longer valid since slow-roll is violated. But we can determine the evolution of γ through the transition using Eq. (23) which, in the $\gamma \gg 1$ limit, reduces to

$$\left[\frac{d\gamma}{dN} \right]_{\pm} \simeq 3\gamma_{\text{sr}}^{(+)}(N_0) \frac{\Delta A}{A_+}. \quad (32)$$

Therefore, during the transition era, the Lorentz factor decreases exponentially (recall that $\Delta A < 0$) and

$$\gamma^{(-)}(N) = \left[\gamma_{\text{sr}}^{(+)}(N_0) - \gamma_{\text{sr}}^{(-)}(N_0) \right] e^{-3(N-N_0)} + \gamma_{\text{sr}}^{(-)}(N) \quad (33)$$

since the continuity of γ requires that $\gamma^{(-)}(N_0) = \gamma_{\text{sr}}^{(+)}(N_0)$, while $\gamma(N \gg N_0) = \gamma_{\text{sr}}^{(-)}(N)$. Once again, this excellent fit for γ is shown in Fig. 2.

We now turn to the behaviour of the slow-roll parameters. The quantity ϵ_1 is determined directly from Eq. (13). Away from the transition, where the slow-roll approximation is valid, one obtains

$$\epsilon_{1\text{sr}}^{(\pm)}(N) \simeq \frac{M_{\text{Pl}} A_\pm}{2V_0} \sqrt{\frac{3}{\lambda V_0}} \phi^2(N), \quad (34)$$

while during the transition Eq. (13) yields

$$\epsilon_1^{(-)}(N) = \left[\epsilon_{1\text{sr}}^{(+)}(N_0) - \epsilon_{1\text{sr}}^{(-)}(N_0) \right] e^{-3(N-N_0)} + \epsilon_{1\text{sr}}^{(-)}(N). \quad (35)$$

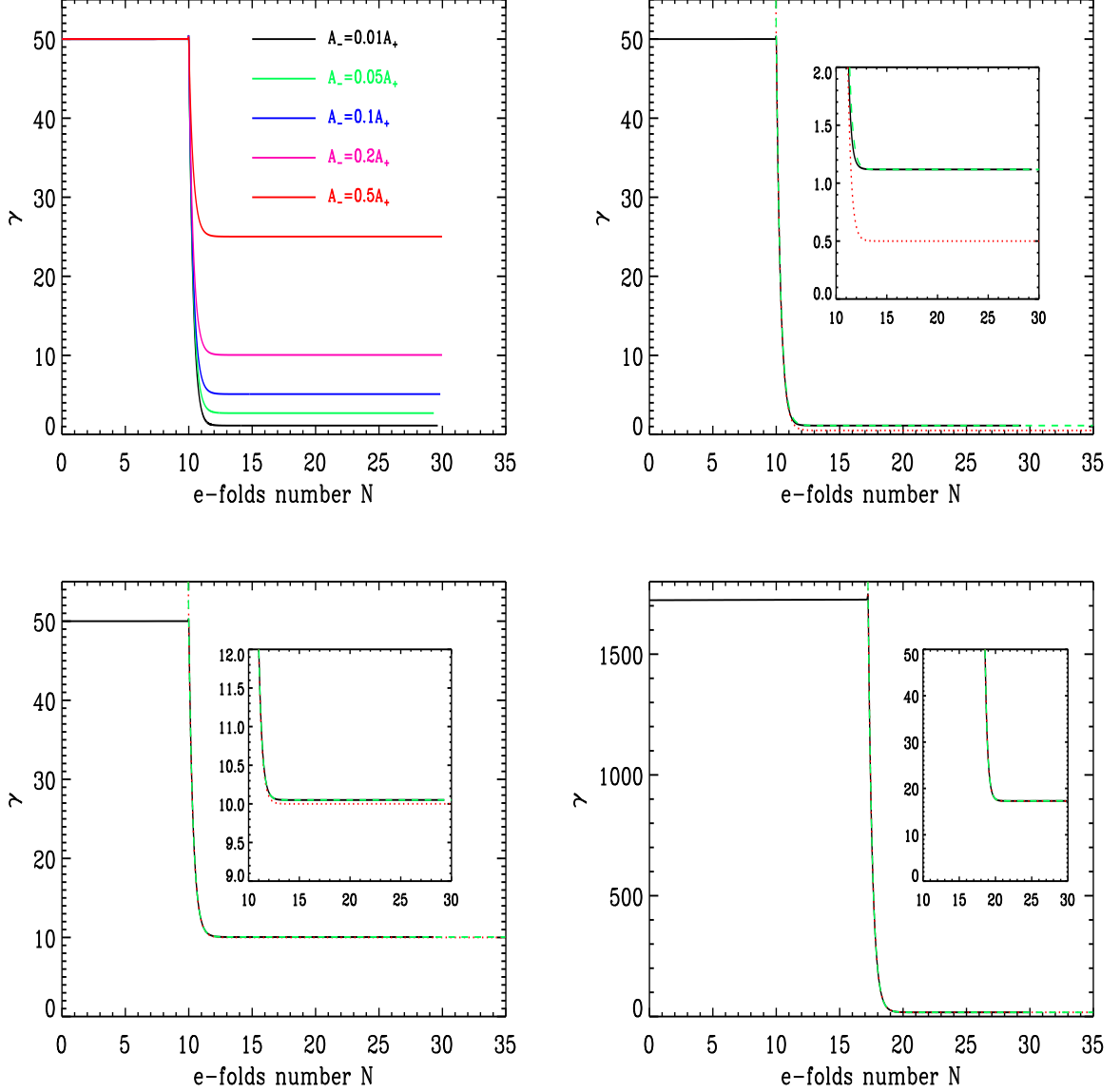


FIG. 2: **Top left panel:** Evolution of the Lorentz factor $\gamma(N)$ for “run one” (see the definition of “run one” in the caption of Fig. 1) for $A_- = 0.01A_+$ (solid black line), $A_- = 0.05A_+$ (solid green line), $A_- = 0.1A_+$ (solid blue line), $A_- = 0.2A_+$ (solid pink line) and $A_- = 0.5A_+$ (solid red line). The transition at $N_0 = 10$ due to the discontinuity in the slope of the potential is clearly visible in this figure. **Top right panel:** “run one” for $A_- = 0.01A_+$ (same as the solid black line in top left panel). The dashed green curve corresponds to the approximate slow-roll evolution of the Lorentz factor given by Eq. (30) and valid after the transition. The dotted red curve corresponds to neglecting the term one inside the square in this expression and, therefore, to assuming that $\gamma_{\text{SR}}(N) = \sqrt{\lambda/(3V_0)} A_- M_{\text{Pl}}/\phi^2(N)$. As shown in the inset, the dashed green line is an excellent fit while the dotted red line is not accurate enough. This is because the case $A_- = 0.01A_+$ corresponds to a brutal change in the slope of the potential such that the field velocity strongly decreases after the transition. As a consequence, the Lorentz factor approaches one and the factor one in the square root in Eq. (30) can no longer be neglected. **Bottom left panel:** same as top right panel but with $A_- = 0.2A_+$. As shown in the inset, this time, both the dashed green line and the dotted red line are good fits of the numerical solution. Clearly, this is because the change of slopes is less abrupt and, therefore, the field velocity decreases less at the transition. As a consequence, the Lorentz factor remains large compared to one and the factor one in the square root in Eq. (30) can now be safely neglected. **Bottom right panel:** same as top right panel but for “run two” (see the definition of “run two” in the caption of Fig. 1). The dashed green line and dotted red line are excellent fit of the actual numerical solution (see the inset) despite the fact that the change in the slopes is abrupt, $A_- = 0.01A_+$. The reason for this behaviour is of course that the initial value of the Lorentz factor is higher.

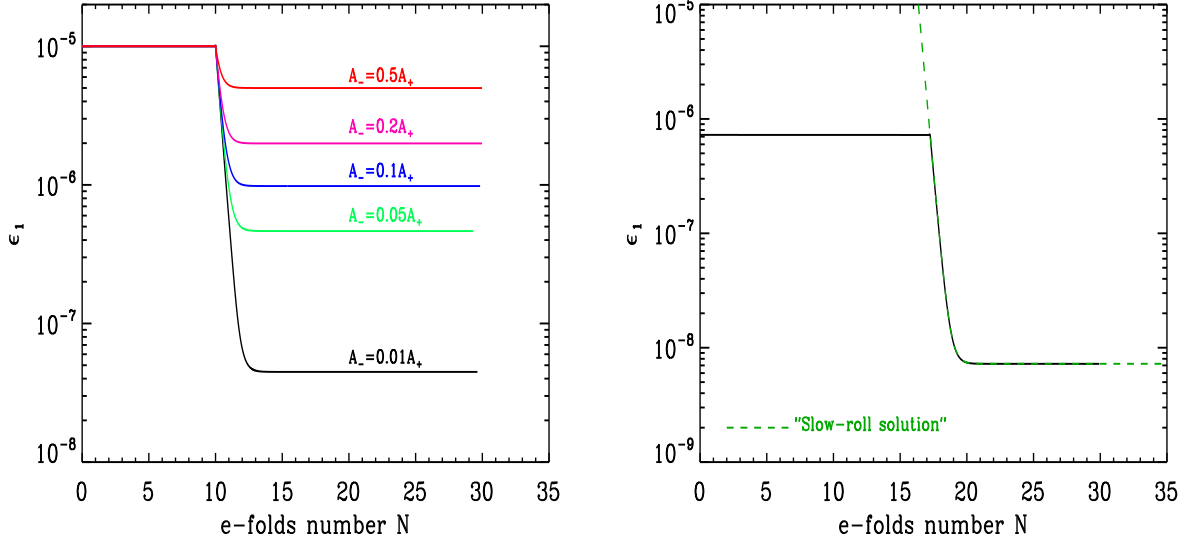


FIG. 3: **Left panel:** Evolution of the first slow-roll parameter ϵ_1 for “run one” (see the definition of “run one” in the caption of Fig. 1) for $A_- = 0.01A_+$ (solid black line), $A_- = 0.05A_+$ (solid green line), $A_- = 0.1A_+$ (solid blue line), $A_- = 0.2A_+$ (solid pink line) and $A_- = 0.5A_+$ (solid red line). **Right panel:** Evolution of the first slow-roll parameter ϵ_1 for “run two” (see the definition of “run two” in the caption of Fig. 1). The dark green dashed line corresponds to the “slow-roll” solution given by Eq. (35) (and valid only after the transition). As can be observed from the figure, this is an excellent fit to the numerical solution.

Thus ϵ_1 also decays exponentially during the transition, from a very small value to another small value: in other words ϵ_1 is small even in the transition region around ϕ_0 . These analytical estimates are compared to the exact evolution of ϵ_1 in Fig. 3 and one again notices that the matching is excellent.

Let us now study the slow-roll parameters δ_1 and ϵ_2 . Upon using Eq. (15), one obtains the following expression valid only far from the transition

$$\delta_{1\text{SR}}(N) \simeq 2\sqrt{\frac{3}{\lambda V_0}}\phi(N). \quad (36)$$

As opposed to ϵ_1 , this slow-roll parameter does not depend on A_{\pm} . During the transition, one has

$$\delta_1^{(-)}(N) = \frac{3\Delta A}{A_-} \frac{e^{-3(N-N_0)}}{1 - (\Delta A/A_-)e^{-3(N-N_0)}} + \delta_{1\text{SR}}(N). \quad (37)$$

The behaviour of the slow-roll parameter ϵ_2 can be obtained in the following way. Starting from Eq. (26) it follows that

$$M_{\text{Pl}}^2 \frac{V_{\phi\phi}}{V} \simeq \frac{\gamma}{2} (4\epsilon_1 - \epsilon_2 - \delta_1). \quad (38)$$

Thus in the slow-roll regimes on either side of ϕ_0 where $V_{\phi\phi} = 0$,

$$4\epsilon_{1\text{SR}}^{(\pm)} = \epsilon_{2\text{SR}}^{(\pm)} + \delta_{1\text{SR}}. \quad (39)$$

On the other hand, we have established that during the transition, $\epsilon_2 \simeq \delta_1$ when $\gamma \gg 1$ [see Eq. (24)]. Thus on combining Eqs. (37) and (39), we find

$$\epsilon_2^{(-)}(N) = \frac{3\Delta A}{A_-} \frac{e^{-3(N-N_0)}}{1 - (\Delta A/A_-)e^{-3(N-N_0)}} + 4\epsilon_{1\text{SR}}^{(-)}(N) - \delta_{1\text{SR}}(N), \quad (40)$$

where $\epsilon_{1\text{SR}}^{(-)}$ and $\delta_{1\text{SR}}$ are given in Eqs. (34) and (36) respectively. The above considerations are checked in Fig. 4 where the above analytical estimates are shown to be excellent approximations to the exact numerical evolutions of the two slow-roll parameters ϵ_2 and δ_1 .

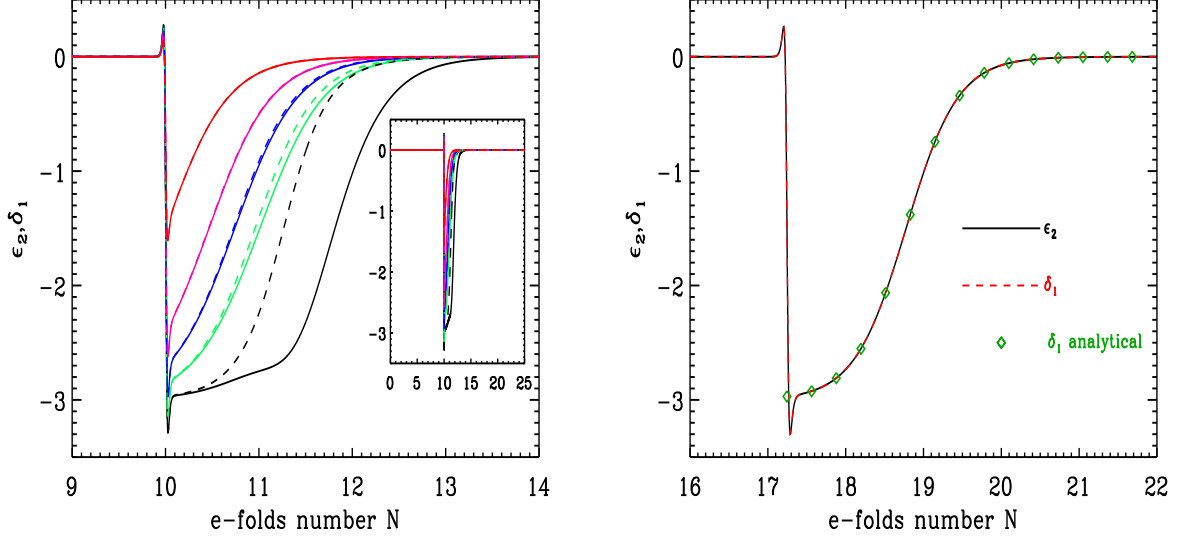


FIG. 4: **Left panel:** evolution of the slow-roll parameters ϵ_2 and δ_1 for “run one” (see the definition of “run one” in the caption of Fig. 1) for $A_- = 0.01A_+$ (solid black line for ϵ_2 and dashed black line for δ_1), $A_- = 0.05A_+$ (solid green line for ϵ_2 and dashed green line for δ_1), $A_- = 0.1A_+$ (solid blue line for ϵ_2 and dashed blue line for δ_1), $A_- = 0.2A_+$ (solid pink line for ϵ_2 and dashed pink line for δ_1) and $A_- = 0.5A_+$ (solid red line for ϵ_2 and dashed red line for δ_1). Outside the region of the transition, around $N_0 = 10$, the evolution is featureless as shown in the inset. When the change in the slope is not too abrupt, one observes that $\epsilon_2 \simeq \delta_1$. Of course the most important result shown in the figure is that ϵ_2 and δ_1 can be large during the transition. When the kinetic term is standard, slow-roll violation corresponds to a situation where $\epsilon_1 \ll 1$ (*i.e.* inflation never stops) and $|\epsilon_2| > 1$. In the DBI case, this situation generalises to $\epsilon_1 \ll 1$, $|\epsilon_2| > 1$ and $|\delta_1| > 1$. **Right panel:** evolution of the slow-roll parameters ϵ_2 and δ_1 for “run two” (see the definition of “run two” in the caption of Fig. 1). In this case we have $\epsilon_2 \simeq \delta_1$ with a very good approximation despite the fact that $A_- = 0.01A_+$. As before, this is due to the fact that the initial velocity of the field is much larger than in the left panel. The dark green dots correspond to the “slow-roll” solution given by Eq. (37) (and valid only after the transition). As can be noticed in the figure, this is an excellent fit to the numerical solution. The small peaks around N_0 are simply numerical artifacts whose origin stems from the fact that we have modelled the Heaviside function with a hyperbolic tangent. The amplitude of these peaks can be decreased at will by increasing the sharpness of the hyperbolic tangent.

Finally, we study the behaviour of the quantities $\delta_1\delta_2$ and $\epsilon_2\epsilon_3$. These two combinations are important because they appear in the effective potential for the cosmological perturbations (see the next section). Just after the discontinuity, where $\epsilon_2 \simeq \delta_1 \gg \epsilon_1$, we find from Eqs. (16) and (17) that

$$\delta_1\delta_2 \simeq -3\delta_1 - \frac{T_{\phi\phi}}{H^2} \simeq -3\epsilon_2 - \epsilon_2^2, \quad (41)$$

$$\epsilon_2\epsilon_3 \simeq -3\epsilon_2 - \epsilon_2^2, \quad (42)$$

where we have neglected the $T_{\phi\phi}$ term in $\delta_1\delta_2$ which is small. Thus, substituting (40) yields the fit after the discontinuity of

$$\delta_1\delta_2 \simeq \epsilon_2\epsilon_3 \simeq -9 \frac{\Delta A}{A_-} \frac{e^{-3(N-N_0)}}{[1 - (\Delta A/A_-)e^{-3(N-N_0)}]^2}. \quad (43)$$

This analytical approximation is tested in Fig. 5. As can be seen in this plot, the matching to the exact numerical solution is excellent.

To summarise, the above considerations show that on assuming that potential is vacuum dominated, that the system is initially in slow-roll, and that $\gamma \gg 1$ for all times, then it is possible to obtain excellent analytical approximations for each relevant background quantities and slow-roll parameters throughout the evolution, despite the fact that slow-roll is violated at the transition. This is important since the slow-roll parameters control the evolution of the time-dependent frequency of each Fourier mode of the perturbations. In the next section we study in detail cosmological fluctuations, our final goal being to determine their power-spectrum. Before doing so, however, we end by noting

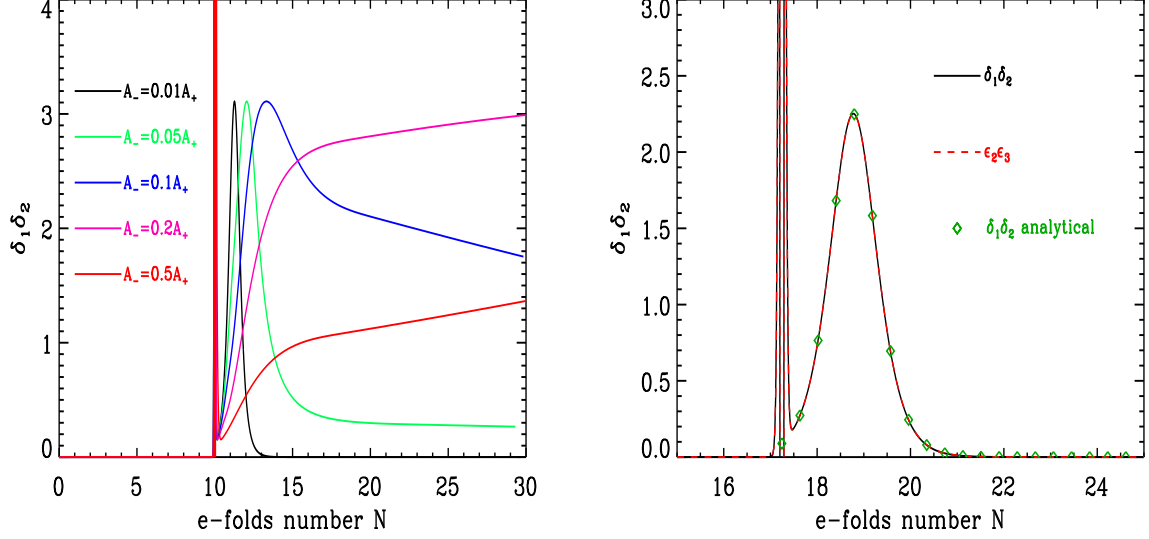


FIG. 5: **Left panel:** evolution of $\delta_1 \delta_2$ for "run one" (see the definition of "run one" in the caption of Fig. 1) for $A_- = 0.01A_+$ (solid black line), $A_- = 0.05A_+$ (solid green line), $A_- = 0.1A_+$ (solid blue line), $A_- = 0.2A_+$ (solid pink line) and $A_- = 0.5A_+$ (solid red line). **Right panel:** evolution of $\delta_1 \delta_2$ (solid black line) and $\epsilon_2 \epsilon_3$ (dashed red line) for "run two" (see the definition of "run two" in the caption of Fig. 1). We observe that $\delta_1 \delta_2 \simeq \epsilon_2 \epsilon_3$. The dark green dots correspond to the "slow-roll" solution given by Eq. (43) (and valid only after the transition). As can be noticed in the figure, this is an excellent fit to the numerical solution. The vertical lines at N_0 originate from the Dirac function in $V_{\phi\phi}$ in Eq. (16).

that in the slow-roll regime far from the discontinuity, $\gamma_{\text{SR}}^{(\pm)}$ as well as all the slow-roll parameters, only depend very weakly on N : indeed they remain essentially constant on either side of the discontinuity (as can be seen in Figs. 1 - 5). The origin of this behaviour is the small variation of ϕ with N as seen in Fig. 1. For this reason, in the following, we will often omit to write the explicit N dependence of the slow-roll parameters in the slow-roll regime. In the above expressions, this amounts to approximating $\phi(N)$ by $\phi(N_0) = \phi_0$, so that for example from (34)

$$\epsilon_{1\text{SR}}^{(\pm)} \simeq \frac{M_{\text{Pl}} A_{\pm}}{2V_0} \sqrt{\frac{3}{\lambda V_0}} \phi_0^2 \quad (44)$$

while from Eqs. (31) and (33)

$$\gamma_{\text{SR}}^{(\pm)} \simeq \sqrt{\frac{\lambda}{3V_0}} \frac{M_{\text{Pl}} A_{\pm}}{\phi_0^2}, \quad \gamma^{(-)}(N) \simeq \gamma_{\text{SR}}^{(-)} \left[\frac{\Delta A}{A_-} e^{-3(N-N_0)} - 1 \right]. \quad (45)$$

Having completed the study of the background, we now turn to the perturbations, in particular to the calculation of the two-point correlation function.

III. POWER-SPECTRUM

In this section, we are interested in scalar perturbations. It is well-known that they can be characterised by a single variable, the so-called Mukhanov-Sasaki quantity, $v(\eta, \mathbf{x})$. Its Fourier amplitude obeys the equation of a parametric oscillator, namely

$$v_{\mathbf{k}}'' + \left(\frac{k^2}{\gamma^2} - \frac{z''}{z} \right) v_{\mathbf{k}} = 0, \quad (46)$$

where the prime now denotes a derivative with respect to conformal time, k denotes the comoving wave number of the Fourier mode under consideration, and z is given by [43]

$$z(\eta) = a(\eta) M_{\text{Pl}} \sqrt{2\epsilon_1} \gamma. \quad (47)$$

The effective potential z''/z which determines the evolution of the scalar perturbations can be determined directly from Eq. (47) and the definition of the slow-roll parameters in Eqs. (8) and (9): its exact expression is

$$\frac{z''}{z} = a^2 H^2 \left[2 - \epsilon_1 + \frac{3}{2}\epsilon_2 + \frac{1}{4}\epsilon_2^2 - \frac{1}{2}\epsilon_1\epsilon_2 + \frac{1}{2}\epsilon_2\epsilon_3 + (3 - \epsilon_1 + \epsilon_2)\delta_1 + \delta_1^2 + \delta_1\delta_2 \right]. \quad (48)$$

(Note that if $\delta_1 = \delta_2 = 0$, this reduces to the SSFI expression, see eg. [6]). Another important difference with respect to conventional inflationary theory is the presence of the term $1/\gamma^2 = c_s^2$ in front of k^2 in Eq. (46), responsible for the fact that perturbations now propagate with a speed c_s different to the speed of light. As a result, the question of how initial conditions are chosen is more subtle — indeed, one usually assumes that the initial state is the adiabatic vacuum for which

$$v_{\mathbf{k}}(\eta) \simeq \frac{1}{\sqrt{2\omega(k, \eta)}} \exp \left[\pm i \int^\eta \omega(k, \tau) d\tau \right], \quad (49)$$

where $\omega^2(k, \eta) \equiv c_s^2 k^2 - z''/z$. The adiabatic approximation is valid if $|Q/\omega^2| \ll 1$ where $Q \equiv 3\omega'^2/(4\omega^2) - \omega''/(2\omega)$. In the standard inflationary context, the modes are initially within the Hubble radius and $\omega \simeq k$. It is then obvious that the Wentzel-Kramers-Brillouin (WKB) approximation is valid. In the DBI case, however, the modes are initially within the sonic scale and $\omega \simeq c_s k$. Because of the non-trivial time-dependence of c_s , it is not obvious that $|Q/\omega^2| \ll 1$. If this is the case, then one simply loses the ability to choose a well-defined and well-motivated initial state. In fact, it is easy to show that, on sub-sonic scales,

$$\frac{Q}{\omega^2} = \frac{a^2 H^2}{2c_s^2 k^2} \left(\delta_1 - \epsilon_1 \delta_1 + \delta_1 \delta_2 + \frac{1}{2}\delta_1^2 \right). \quad (50)$$

We have seen that, in the DBI-Starobinsky model, all the slow-roll parameters are small initially (*i.e.* far from the transition). It follows that, in this model, one can identify a well-defined initial state $v_{\mathbf{k}}(\eta) = \gamma/(2k) e^{\pm i k \eta / \gamma}$. This choice is made in the remainder of this article.

The power-spectrum, or two-point correlation function, is defined by

$$\mathcal{P}_\zeta \equiv \frac{k^3}{2\pi^2} |\zeta_{\mathbf{k}}|^2 = \frac{k^3}{4\pi^2} \frac{c_s^2 |v_{\mathbf{k}}|^2}{M_{\text{Pl}}^2 a^2 \epsilon_1}, \quad (51)$$

where $\zeta_{\mathbf{k}} \equiv v_{\mathbf{k}}/z$ is the curvature perturbation, and the right hand side is evaluated in the limit, $k c_s / (aH) \simeq -k\eta/\gamma \rightarrow 0$. To find $\mathcal{P}_\zeta(k)$, we must integrate (46) for each mode starting from the initial conditions discussed above. In general this cannot be done analytically due to the complexity of the equations. As a result, one possibility is to integrate the system numerically, and for this purpose we have written a numerical code which exactly integrates the background and the perturbations mode by mode (and for arbitrary values of the parameters of the model, and hence any c_s). The result is displayed in Fig. 6 (solid blue line). We see that, as k increases, the power-spectrum rapidly dips and reaches its minimum at a scale k_* which is a large multiple of $k_0 \equiv -1/\eta_0$ (namely the mode which left the Hubble radius at $\phi = \phi_0$).¹ This dip is followed by large amplitude, high frequency oscillations. Notice that for the parameters chosen in Fig. 6, the power-spectrum takes the same scale-invariant value on large and small scales. In the conclusion, we will compare this power-spectrum with that obtained in the canonical Starobinsky model for precisely the same values of A_\pm : as we will see, although the shapes share the same general aspect, they are in fact very different.

It is also interesting to have an analytical expression for the power spectrum since this can help understand how its shape is modified when the parameters of the model are changed. Therefore we now aim to develop approximation methods in order to address this question. To solve Eq. (46) and hence determine the $v_{\mathbf{k}}$ and $\mathcal{P}_\zeta(k)$, we use the results of section II B in which the slow-roll parameters were determined as a function of N , and hence as a function of conformal time η since $\eta = \eta_0 e^{-(N-N_0)}$. Our analytical approximation will therefore only be valid in the $c_s \ll 1$ regime for which the results of section II B hold. Before the transition $\eta < \eta_0$, the slow-roll parameters are small and Eq. (48) reduces to $z''/z \simeq 2a^2 H^2 \simeq 2/\eta^2$ so that the solution of (46) is

$$v_{\mathbf{k}}^+(\eta) = \sqrt{\frac{\gamma_{\text{SR}}^{(+)}}{2k}} \left(1 - i \frac{\gamma_{\text{SR}}^{(+)}}{k\eta} \right) e^{-ik\eta/\gamma_{\text{SR}}^{(+)}} \quad (52)$$

¹ Notice that we have chosen to define k_0 without any factor of γ despite the fact that, physically, the relevant scale is aH/c_s . The reason for this is that, in this model, γ varies significantly with time and it is not very convenient to include it in the definition of the preferred scale.

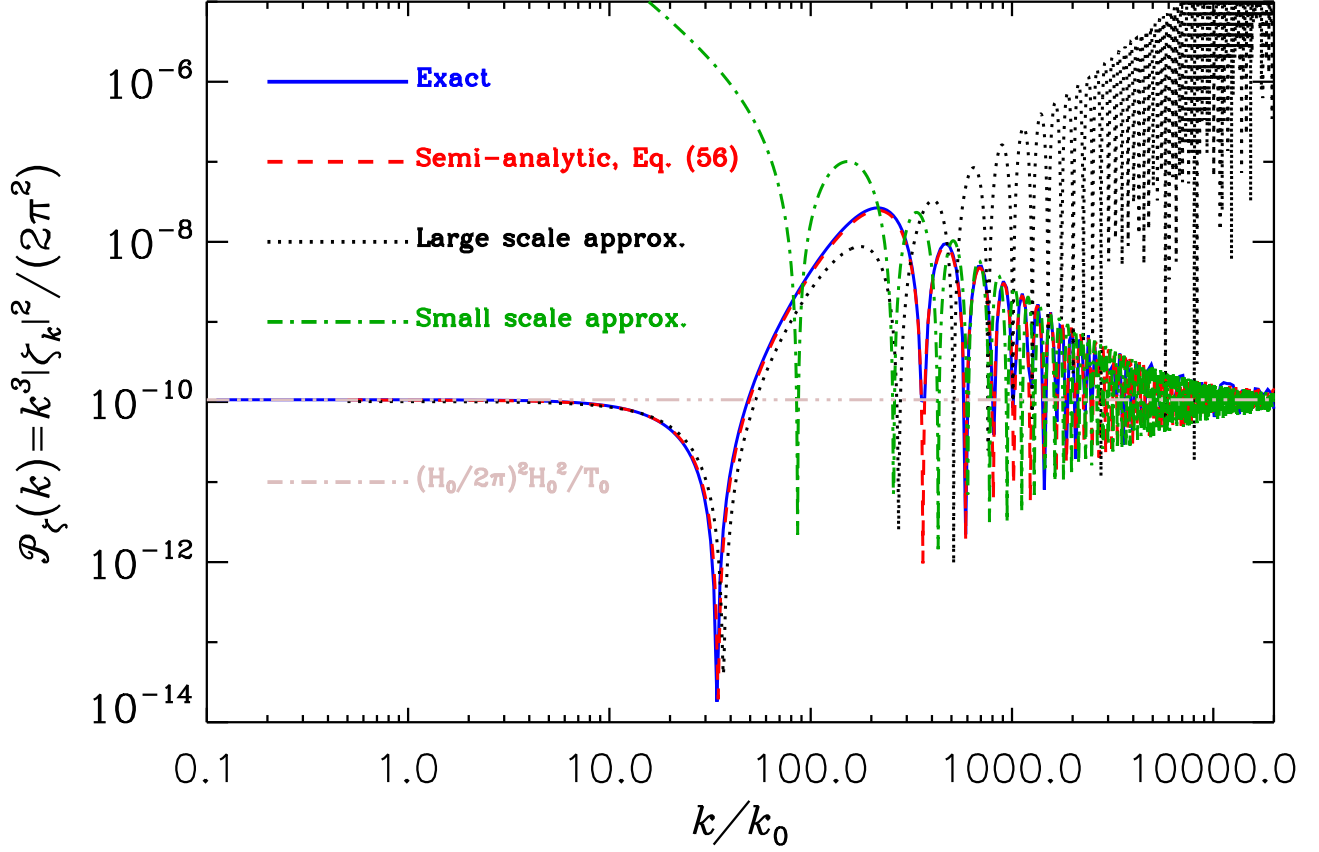


FIG. 6: Power spectrum of the DBI-Starobinsky model and various approximations. The solid blue line represents the exact power spectrum obtained with a numerical, mode by mode, integration for “run two”. The dashed red line gives \mathcal{P}_ζ obtained from an integration of Eq. (55). The dotted black line corresponds to the power spectrum derived from Eq. (62) and is valid only in the large scale limit while the dotted dashed green line comes from Eq. (60) and is relevant only in the small scale limit. Finally, the grey horizontal line gives the asymptotic values of the power spectrum, see Eqs. (66) and (64).

where $\gamma_{\text{SR}}^{(+)}$ is given in Eq. (45). After the transition, the effective potential z''/z can be calculated using the fact that $\delta_1 \simeq \epsilon_2 \gg \epsilon_1$ while $\delta_1 \delta_2$ and $\epsilon_1 \epsilon_2$ are given in Eq. (41) and (42) respectively. On substituting, one finds that the terms linear in slow-roll parameters in (48) cancel (just as in the canonical Starobinsky model), but the quadratic terms do not, resulting in $z''/z \simeq \mathcal{H}^2(2 + 3\epsilon_2^2/4)$. Thus after the transition, the mode function satisfies

$$v_{\mathbf{k}}^{-''} + \left\{ \frac{k^2}{\gamma^2(\eta)} - \frac{1}{\eta^2} \left[2 + \frac{3}{4} \epsilon_2^2(\eta) \right] \right\} v_{\mathbf{k}}^- = 0, \quad (53)$$

where, from Eq. (40)

$$\epsilon_2 = \epsilon_2^{(-)} \simeq \frac{3\Delta A}{A_-} \frac{e^{-3(N-N_0)}}{1 - (\Delta A/A_-)e^{-3(N-N_0)}} = 3 \frac{\tilde{\omega} \eta^3}{(1 - \tilde{\omega} \eta^3)} \quad (54)$$

with $\tilde{\omega} \equiv (\Delta A/A_-)/\eta_0^3 > 0$. Thus, on using Eq. (45), we finally arrive at

$$v_{\mathbf{k}}^{-''} + \left[\frac{k^2}{\left(\gamma_{\text{SR}}^{(-)} \right)^2 (1 - \tilde{\omega} \eta^3)^2} - \frac{2}{\eta^2} - \frac{27}{4} \frac{\tilde{\omega}^2 \eta^4}{(1 - \tilde{\omega} \eta^3)^2} \right] v_{\mathbf{k}}^- = 0. \quad (55)$$

This equation is one of the central results of this paper, since the power-spectrum is determined directly from its solution. In order to find $\mathcal{P}_\zeta(k)$, the modes $v_{\mathbf{k}}^\pm$ and their derivatives must be matched at $\eta = \eta_0 = -1/(a_0 H_0)$ [so

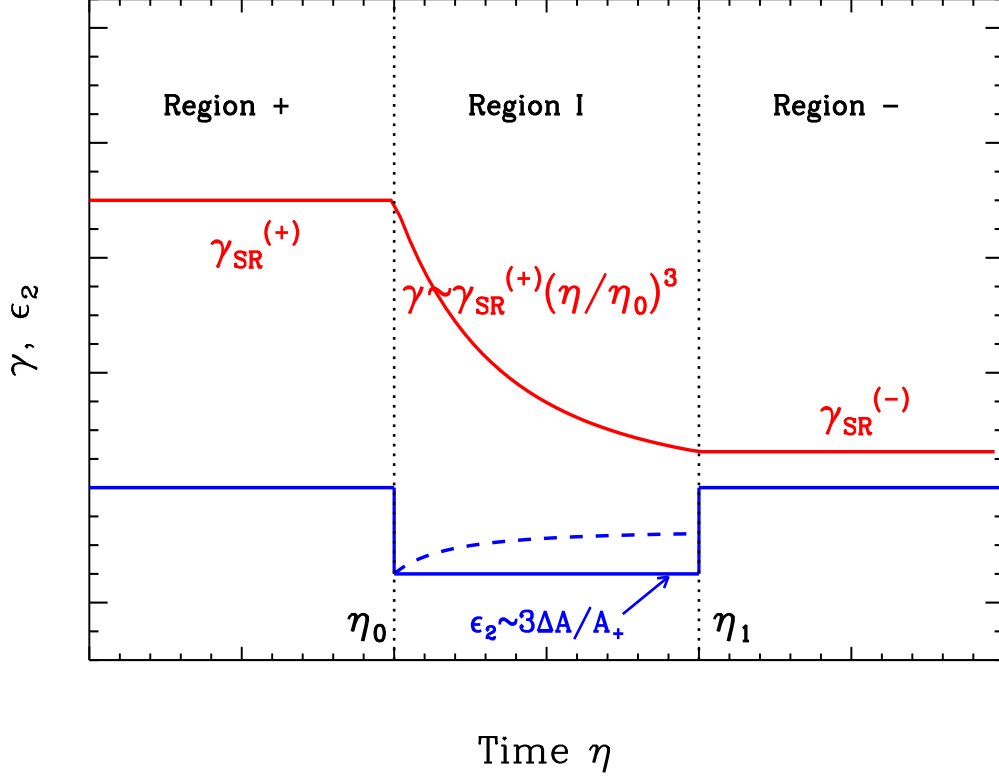


FIG. 7: Approximations for an analytic solution of the mode equation (55). Solid lines: approximations for γ (red) and ϵ_2 (blue) made on small scales. On large scales, the η -dependence of ϵ_2 is taken into account (dashed line), namely from Eq. (40), $\epsilon_2 \simeq (3\Delta A/A_-)e^{-3(N-N_0)} / [1 - (\Delta A/A_-)e^{-3(N-N_0)}]$.

as to determine the two integration constants associated with Eq. (55)]. This can be done by carefully considering of the behaviour of z and z''/z across the transition. Indeed, on recalling that $z = M_{\text{Pl}}a(\eta)\sqrt{2\epsilon_1(\eta)}\gamma(\eta)$, and using Eqs. (33) and (35), one finds

$$\frac{z''}{z} \simeq -\frac{9}{2} \frac{\Delta A}{A_+} \frac{1}{\eta_0} \delta^{(1)}(\eta - \eta_0) = a_0 H_0 \frac{9}{2} \frac{\Delta A}{A_+} \delta^{(1)}(\eta - \eta_0). \quad (56)$$

Hence the matching conditions at the transition are

$$v_{\mathbf{k}}^-(\eta_0) = v_{\mathbf{k}}^+(\eta_0), \quad v_{\mathbf{k}}'^-(\eta_0) - v_{\mathbf{k}}'^+(\eta_0) = a_0 H_0 \frac{9}{2} \frac{\Delta A}{A_+} v_{\mathbf{k}}^-(\eta_0). \quad (57)$$

Unfortunately, Eq. (55) is not soluble analytically. However, it can be solved numerically. At this point, one could wonder whether we have gained something given that our aim was to derive approximate analytical formulae and that we have already determined \mathcal{P}_ζ exactly by means of a mode by mode integration. However, integrating a single differential equation is much easier than writing a mode by mode numerical code and, moreover, as we will discuss below, Eq. (55) can also be approximated analytically. In Fig. 6 we plot the power-spectrum obtained by solving (55) numerically, and then substituting into (51) (red dashed curve). This is compared with the fully mode by mode numerical calculation of the power-spectrum (solid blue line) obtained by solving both the background and perturbation equations numerically. The agreement is excellent, thus validating all the reasoning used to arrive at (55).

Our aim is now to determine analytically the dependence of the features described above on the parameters of the model A_\pm . The correct behaviour of $\mathcal{P}_\zeta(k)$ on small and large scales can be captured analytically via the following approximation scheme. First introduce a conformal time $\eta_1 > \eta_0$ so that the period after the transition is split into

two parts, see Fig. 7. When $\eta \geq \eta_1$, which we denote by ‘region $-$ ’, we take $\epsilon_2 \simeq 0$ and $\gamma = \gamma_{\text{SR}}^{(-)}$. The solution of Eq. (53) is then particularly straightforward, namely

$$v_{\mathbf{k}}^- = \alpha_{\mathbf{k}} \sqrt{\frac{\gamma_{\text{SR}}^{(-)}}{2k}} \left(1 - i \frac{\gamma_{\text{SR}}^{(-)}}{k\eta} \right) e^{-ik\eta/\gamma_{\text{SR}}^{(-)}} + \beta_{\mathbf{k}} \sqrt{\frac{\gamma_{\text{SR}}^{(-)}}{2k}} \left(1 + i \frac{\gamma_{\text{SR}}^{(-)}}{k\eta} \right) e^{ik\eta/\gamma_{\text{SR}}^{(-)}}. \quad (58)$$

The integration constants $\alpha_{\mathbf{k}}$ and $\beta_{\mathbf{k}}$, to be calculated below, determine the power-spectrum since from Eq. (51) it follows that

$$\mathcal{P}_\zeta(k) = \frac{H_-^2}{8\pi^2 M_{\text{Pl}}^2} \frac{\gamma_{\text{SR}}^{(-)}}{\epsilon_1} |\beta_{\mathbf{k}} - \alpha_{\mathbf{k}}|^2 = \left(\frac{H_0}{2\pi} \right)^2 \left(\frac{H_0^2}{T_0} \right) |\beta_{\mathbf{k}} - \alpha_{\mathbf{k}}|^2 \quad (59)$$

where $T_0 = T(\phi_0)$. In the intermediate region, “region I” for which $\eta_0 \leq \eta < \eta_1$, we make the following assumptions (see Fig. 7). On small scales, we assume ϵ_2 constant, with $\epsilon_2 \simeq \epsilon_2(\eta_0) = 3\Delta A/A_+$ as obtained from Eq. (40), while from Eq. (33) the evolution of $\gamma(\eta)$ is approximated by $\gamma \simeq \gamma_{\text{SR}}^{(+)} (\eta/\eta_0)^3$. Continuity of γ at η_1 determines η_1 to be given by $\eta_1 = \eta_0 (\gamma_{\text{SR}}^{(-)}/\gamma_{\text{SR}}^{(+)})^{1/3}$. In that case, Eq. (53) has the exact solution

$$v_{\mathbf{k},\text{small}}^{\text{I}} = \sqrt{\frac{\eta}{\eta_1}} \left[\tilde{C}_1(k) J_\nu(x) + \tilde{C}_2(k) Y_\nu(x) \right] \quad (60)$$

where $\tilde{C}_1(k), \tilde{C}_2(k)$ are k -dependent integration constants, and

$$x(\eta, k) \equiv \frac{1}{2} \left(\frac{k\eta_0}{\gamma_{\text{SR}}^{(+)}} \right) \left(\frac{\eta_0}{\eta} \right)^2, \quad \nu \equiv \frac{3}{4} \sqrt{1 + 3 \left(\frac{\Delta A}{A_+} \right)^2}. \quad (61)$$

In the intermediate region and on large scales, our assumptions are slightly different. Since $\gamma \gg 1$, here we expect $k^2/\gamma^2 \ll 1$, and hence we simply first neglect this term Eq. (55), while keeping the exact η -dependence of ϵ_2 . We can then integrate exactly to find

$$v_{\mathbf{k},\text{large}}^{\text{I}} = \frac{\tilde{C}_3(k)}{\eta} + \tilde{C}_4(k) \eta^2 (-2 + \tilde{\omega} \eta^3) \quad (62)$$

where $\tilde{C}_3(k)$ and $\tilde{C}_4(k)$ are again k -dependent integration constants. The different integration constants $\tilde{C}_i(k)$, $i = 1, \dots, 4$ are determined from the boundary conditions at η_0 which, from Eq. (57), read

$$v_{\mathbf{k}}^{\text{I}}(\eta_0) = v_{\mathbf{k}}^+(\eta_0), \quad v_{\mathbf{k}}^{\text{I}'}(\eta_0) - v_{\mathbf{k}}^{+'}(\eta_0) = a_0 H_0 \frac{9}{2} \frac{\Delta A}{A_+} v_{\mathbf{k}}^+(\eta_0), \quad (63)$$

where the mode solutions in the “ $+$ ” region, $v_{\mathbf{k}}^+$, are given in Eq. (52). In turn, the integration constants $\alpha_{\mathbf{k}}$ and $\beta_{\mathbf{k}}$ are then obtained from matching at η_1 , where the relevant conditions are $v_{\mathbf{k}}^{\text{I}}(\eta_1) = v_{\mathbf{k}}^-(\eta_1)$ and $v_{\mathbf{k}}^{\text{I}'}(\eta_1) = v_{\mathbf{k}}^{-'}(\eta_1)$, namely the mode functions and their derivatives are continuous. Finally, the power-spectrum $\mathcal{P}_\zeta(k)$ is then obtained from Eq. (59).

Carrying out this process on large scales using (62) gives an analytic expression for $\mathcal{P}_\zeta(k)$, which is plotted in Fig. 6 (dotted black line). As can be seen, this is good fit to the full numerical solution (solid blue line) on large scales. Since the analytical expression is somewhat long, and so we do not give it explicitly — however, we can use it to extract the dependence of $\mathcal{P}_\zeta(k)$ on the parameters of the model. In particular, we find that

$$\lim_{k/k_0 \rightarrow 0} \mathcal{P}_\zeta(k) = \left(\frac{H_0}{2\pi} \right)^2 \left(\frac{H_0^2}{T_0} \right) \left[\left(1 - \frac{A_-}{2A_+} \right) \left(1 + \frac{A_-}{A_+} \right)^2 \right] \quad (64)$$

which agrees very well with the numerical values found for different A_\pm . Notice that when $A_-/A_+ \rightarrow 0$, on large scales the power-spectrum tends to the asymptotic scale invariant value $(H_0/2\pi)^2 (H_0^2/T_0)$, drawn by a grey dotted-dotted-dashed line in Fig. 6. With our analytic approximation for $\mathcal{P}_\zeta(k)$, one can also determine the position of the first feature in the power-spectrum, namely the smallest value of $k = k_*$ for which $\mathcal{P}_\zeta(k_*) \rightarrow 0$. This reduces to solving an implicit equation of the form $\tan(k_* \eta_1 / \gamma_{\text{SR}}^{(-)}) = f(k_* \eta_1 / \gamma_{\text{SR}}^{(-)})$ where the function $f(x)$ is a ratio of two polynomials, determined straightforwardly from the matching, and with A_\pm dependent coefficients. One can check

that the analytic result agrees well with that obtained from a numerical solution of the full power-spectrum. It can be approximated by

$$\frac{k_*}{k_0} \simeq \left(\frac{A_+}{A_-} \right)^{0.81} \quad (65)$$

thus showing the dependence on A_{\pm} : the larger A_-/A_+ the more the feature shifts to large scales.

Once again, carrying out the same procedure on small scales using (60), we again determine an analytic expression for $\mathcal{P}_{\zeta}(k)$ now containing Bessel functions (which are responsible for the oscillations in the power-spectrum). Again the expression is rather complicated, but it is a good fit to the numerical result (see Fig 6, dotted dashed green line). We can use it to extract the $k \rightarrow \infty$ behaviour of the power-spectrum (this limit is particularly simple since then the arguments of the Bessel functions are large, and they can be replaced by their appropriate asymptotic expansions). We find that the scale invariant value of the power-spectrum on small scales is given by

$$\lim_{k/k_0 \rightarrow \infty} \mathcal{P}_{\zeta}(k) = \left(\frac{H_0}{2\pi} \right)^2 \left(\frac{H_0^2}{T_0} \right) \quad (66)$$

as advertised in the introduction, and also shown in Fig. 6. We can go further: when $A_- \ll A_+$ it follows that $\nu \simeq 3/2$ and then the exact expressions for the Bessel functions are known. Our analytic result then gives

$$\mathcal{P}_{\zeta}^{(A_- \ll A_+)}(k) = \left(\frac{H_0}{2\pi} \right)^2 \left(\frac{H_0^2}{T_0} \right) \left\{ 1 + \left(\frac{3\gamma_{\text{SR}}^{(+)}}{k\eta_0} \right) \sin[2\theta(k)] + \left(\frac{3\gamma_{\text{SR}}^{(+)}}{k\eta_0} \right)^2 \cos^2[\theta(k)] \right\} \quad (\text{for } k \gg k_0) \quad (67)$$

where

$$\theta(k) = \frac{1}{2} \left(\frac{k\eta_0}{\gamma_{\text{SR}}^{(+)}} \right) \left[3 \left(\frac{\gamma_{\text{SR}}^{(+)}}{\gamma_{\text{SR}}^{(-)}} \right)^{2/3} - 1 \right] \simeq \frac{3}{2} \left(\frac{k\eta_0}{\gamma_{\text{SR}}^{(+)}} \right) \left(\frac{\gamma_{\text{SR}}^{(+)}}{\gamma_{\text{SR}}^{(-)}} \right)^{2/3} \quad \text{for } \gamma_{\text{SR}}^{(+)} \gg \gamma_{\text{SR}}^{(-)}. \quad (68)$$

Thus the wavelength of the oscillations is approximately given by $\sim \gamma_{\text{SR}}^{(+)} (\gamma_{\text{SR}}^{(-)}/\gamma_{\text{SR}}^{(+)})^{2/3}$ and depends on A_{\pm} through the dependence of $\gamma_{\text{SR}}^{(\pm)}$ on these parameters. Relative to the asymptotic value of $\mathcal{P}_{\zeta}(k \rightarrow \infty)$, the amplitude of these oscillations is determined by the ratio $3\gamma_{\text{SR}}^{(+)}k_0/k$. When $3\gamma_{\text{SR}}^{(+)}k_0/k > 1$, it is quadratic in this parameter, while when $3\gamma_{\text{SR}}^{(+)}k_0/k < 1$, it is linear. This can be observed in Fig. 6 where, for $k/k_0 \simeq 3\gamma_{\text{SR}}^{(+)} \simeq 5 \times 10^3$, the slope of the envelope can be seen to change.

IV. DISCUSSION AND CONCLUSIONS

The main purpose of this paper was to study the signatures of the inflationary DBI-Starobinsky model, for which the potential is linear with a sharp change in slope at a certain ϕ_0 and the kinetic term a non-minimal, DBI, one. In the case of canonical inflation with such a potential, both the power-spectrum $\mathcal{P}_{\zeta}(k)$ as well as the bi-spectrum are exactly soluble analytically [6, 7]. Here we have addressed the following questions: what is the shape of $\mathcal{P}_{\zeta}(k)$ in the DBI-Starobinsky case? What signature do the non-linear kinetic terms leave? Does $\mathcal{P}_{\zeta}(k)$ still rise sharply from small to large scales?

To approach this problem, first we studied the homogeneous background evolution of the field and generalised slow-roll parameters. We showed in section II B that in the DBI regime $\gamma \gg 1$, these quantities can all be determined analytically to very high accuracy. We also showed that this model is characterised by a first slow-roll parameter ϵ_1 which is tiny throughout the evolution of the system, while the other generalised slow-roll parameters all become large after the transition at ϕ_0 , decaying back to small values over a few e-folds. Armed with the analytical expressions for the slow-roll parameters, we showed that the power-spectrum can simply be obtained by solving the mode equation (55). Furthermore, a numerical solution of this equation was shown to agree exactly with a fully numerical determination of the power-spectrum of the model (both at the back-ground and perturbative level), see Fig. 6.

It is also interesting to compare our results to the predictions of the canonical Starobinsky model, see Fig. 8. Following an analytical approximation of Eq. (55), we were able to show that in the DBI Starobinsky model, it is actually the second dimensionful potential $T(\phi)$ (rather than A_{\pm}) which determines the power-spectrum on small and large scales, as summarised in Eqs. (64) and (66). Thus as opposed to the canonical Starobinsky model in which there is a sharp rise in power across k_0 if $A_- \ll A_+$, in the DBI-Starobinsky model there is *no* rise in power in

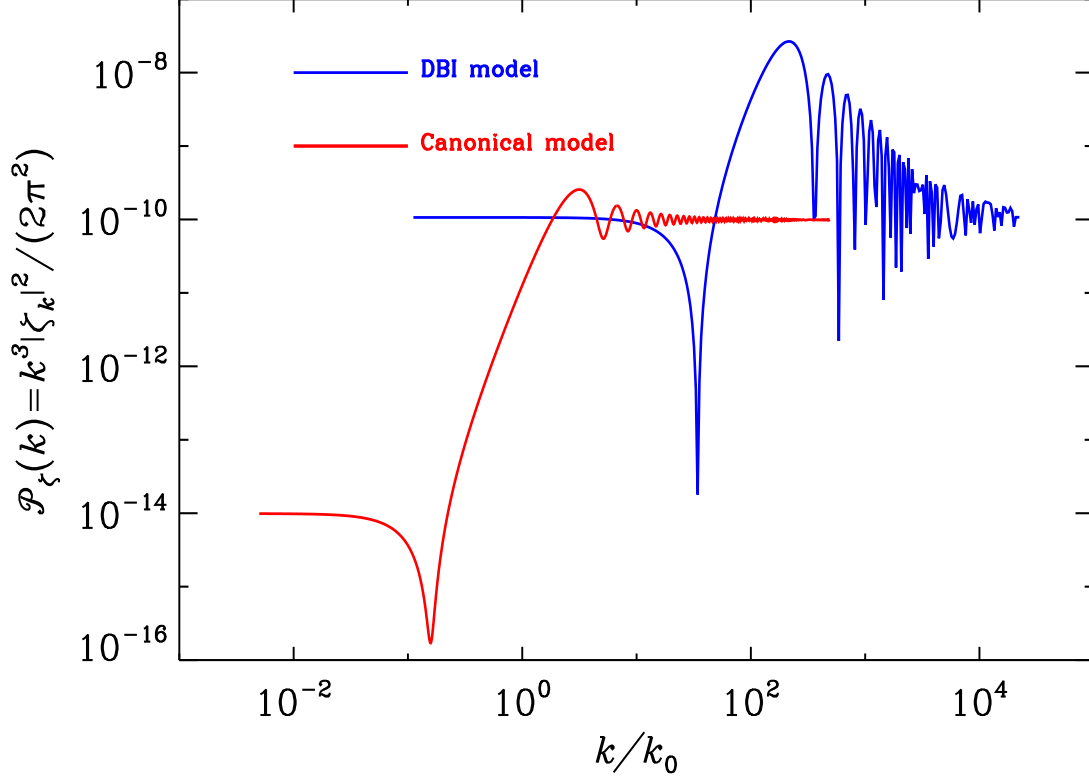


FIG. 8: Comparison of the DBI-Starobinsky and CS-Starobinsky power spectra for the same values of A_+ and A_- corresponding to “run two”. Obviously, the amplitude of the oscillations is much smaller in the CS-Starobinsky case but there is a rise in power that does not exist in the DBI-Starobinsky power spectrum.

this case, see Fig. 8. We were also able to determine the position of the first feature in the power-spectrum, given to a good approximation by $k_*/k_0 \simeq (A_+/A_-)^p$ with $p \sim 0.8$. Again this differs from the CS model in which this feature is at $k_* \simeq k_0$, independently of A_{\pm} . Finally, in the $A_- \ll A_+$ limit, we have shown that the wavelength of oscillations in the power-spectrum does depend on A_{\pm} , as opposed to the CS model, see Fig. 8. Furthermore, relative to the asymptotic value of $\mathcal{P}_\zeta(k \rightarrow \infty)$, the amplitude of oscillations is now much larger — rather than being of order $|\Delta A/A_+| \sim 1$ (in the CS model), it is now of order $\gamma_{\text{sr}}^{(+)} \gg 1$.

The next step would obviously be to compare in detail the DBI-Starobinsky model to CMB data, and particularly the recently released Planck data. This would require interfacing the numerical code used in this paper to calculate the power spectrum to a CMB code (typically the **CAMB** code [44]), and then in turn to a code allowing us to explore the corresponding parameter space (typically the **COSMOMC** code [45]). Moreover, we would also need to include in the analysis the constraints coming from the higher correlation functions (see below). Clearly, this is beyond the scope of the present article since, here, we mainly focus on the physical properties of the system rather than on data analysis. It is interesting, however, to have a broad idea about the physical values of the parameters. To this aim, we have represented in Fig. 9 the Planck “step model” best fit (solid blue line) [1] with the DBI-Starobinsky power spectrum (solid red line) with $\gamma_{\text{in}} \simeq 5$ and $A_- \simeq 0.92A_+$. Notice that we are now, therefore, in a very different regime to that discussed above since A_+ is similar to A_- and γ is not very large. In this plot, the overall normalisation is arbitrary (we have normalised the two spectra differently on purpose in order to make easier the comparison of the two shapes). Notice that the x-axis is now the physical k today and, hence, the position of the first feature is essentially arbitrary. In particular, it will depend on the post-inflationary evolution. On the other hand, Fig. 9 also indicates that the shape of the DBI-power spectrum is not the same as the CS-Starobinsky model and, as a consequence, a rigorous Bayesian exploration of the parameter space of this model seems to be required before one can conclude whether the model is ruled out or, on the contrary, whether it could explain the Planck anomalies and, therefore, improve the fit. In any case, from the above discussion, it is clear that the ratio A_+/A_- cannot be too different from one otherwise the

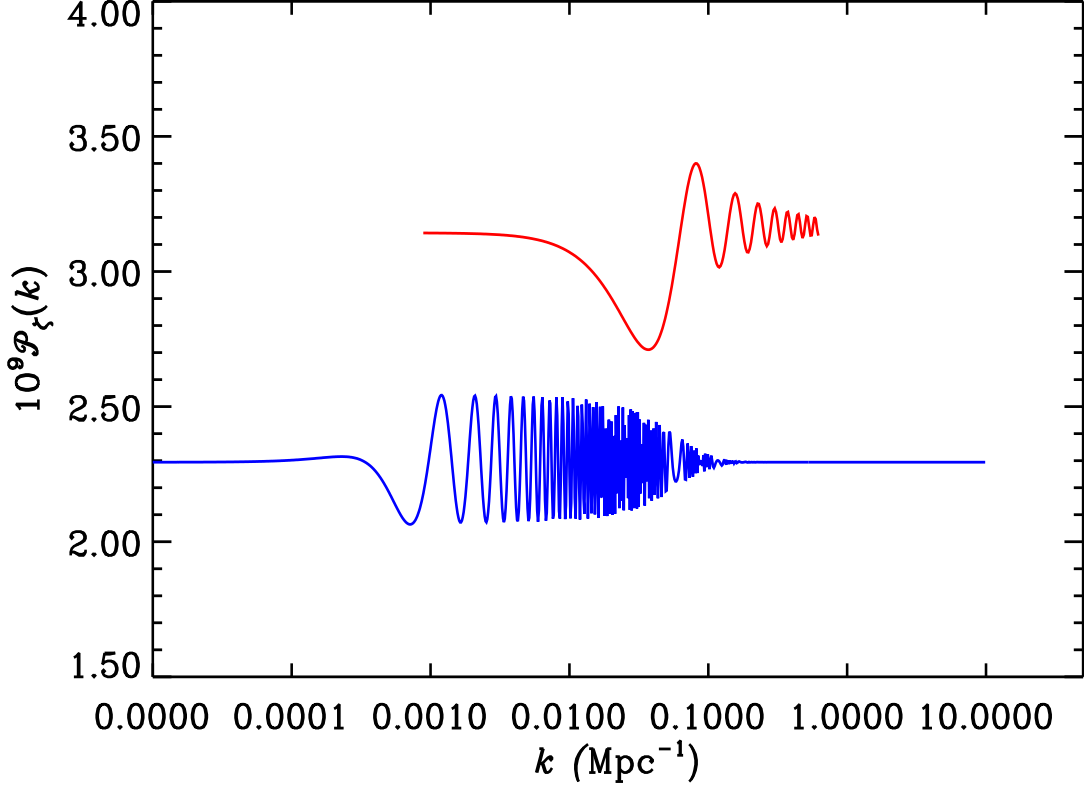


FIG. 9: Comparison of the DBI-Starobinsky power spectrum (solid red line) with the Planck “step-inflation” model best fit (solid blue line). It should be noticed that the DBI-Starobinsky power spectrum normalisation is arbitrary. The DBI-Starobinsky model corresponds to $\epsilon_{1\text{in}} \simeq 10^{-5}$, $\epsilon_{2\text{in}} \simeq 2.5 \times 10^{-5}$, $\delta_{1\text{in}} \simeq 1. \times 10^{-4}$, $\gamma_{\text{in}} \simeq 5$, $\phi_{\text{in}}/M_{\text{Pl}} \simeq 77.4193$, $H_{\text{in}}/M_{\text{Pl}} \simeq 8.88 \times 10^{-7}$ and $N_0 = 10$, where N_0 is the number of e-folds at which the field goes through the transition. This implies $\lambda \simeq 1.09 \times 10^{25}$, $\phi_0/M_{\text{Pl}} \simeq 77.3989$ and $A_+/M_{\text{Pl}}^3 \simeq 2.368 \times 10^{-14}$ and $A_- = 0.92A_+$. To make the comparison easier we have considered $n_s = 1$ for the Planck best fit while it is in fact $n_s \simeq 0.96$. Notice that working with non-negligible values of ϵ_1 and/or ϵ_2 in the DBI Starobinsky model would lead to a significant tilt of the spectrum.

amplitude of the oscillations would obviously be too large (compare for instance Figs. 6 and 9). In addition, γ should not be too large. This has important implications for the exploration of the parameter space since it means that the relevant regime is in fact the “non-perturbative” one *i.e.* the one in which the analytical expressions derived above are no longer applicable. In this situation, only our mode by mode code can be used to explore the compatibility of the model with the data.

Of course, another interesting aspect of the model is to which extent it produces non-Gaussianities. As is well-known, for slow-roll single field inflation with a standard kinetic term, the level of non-Gaussianity is very small, of the order of the slow-roll parameters, see Refs. [46–52]. In the case of the DBI-Starobinsky model, this is obviously no longer true. An interesting feature of the model is that, a priori, non-Gaussianities arise not only from one term, as is usually the case for non-slow-roll models, but from two (or even various) origins: the fact that the kinetic term is non standard and the discontinuity of the derivative of $V(\phi)$ are the main sources of non-Gaussianity in this scenario. Concretely, the third order action reads [42, 53]

$$S_3 = M_{\text{Pl}}^2 \int d\eta d\mathbf{x} \left[-\frac{2a}{3Hc_s^2} \left(-\frac{\epsilon_1 \delta_1}{3c_s^2 \epsilon_X} + u \right) \zeta'^3 + \frac{a^2 \epsilon_1}{c_s^2} \left(\frac{\epsilon_1}{c_s^2} + 3u \right) \zeta \zeta'^2 + \frac{a^2}{2} \frac{\epsilon_1}{c_s^2} \left(\frac{\epsilon_2}{c_s^2} \right)' \zeta^2 \zeta' \right. \\ \left. + \frac{\epsilon_1}{2} \zeta \delta^{ip} \delta^{jq} \partial_i \partial_j \chi \partial_p \partial_q \chi - 2a \frac{\epsilon_1}{c_s^2} \zeta' \delta^{ip} \partial_i \zeta \partial_p \chi - \frac{a^2}{2} \frac{\epsilon_1^3}{c_s^2} \zeta \zeta'^2 + \frac{a^2 \epsilon_1}{c_s^2} (\epsilon_1 + 2\delta_1 - u c_s^2) \delta^{ij} \partial_i \zeta \partial_j \zeta \right], \quad (69)$$

with $\chi \equiv \partial^{-2} [a \Sigma \zeta' / (H^2 M_{\text{Pl}}^2)]$, $\Sigma \equiv \epsilon_1 H^2 M_{\text{Pl}}^2 / c_s^2$ and $\epsilon_X \equiv -\dot{X}/H^2 (\partial H / \partial X)$. The parameter u is defined by $u = 1 - 1/c_s^2$. In slow-roll canonical inflation, the first vertex is absent because $u = \delta_1 = 0$. In DBI inflation, this

is no longer the case and it gives rise to non-vanishing non-Gaussianities with $f_{\text{NL}}^{\text{eq}} \simeq 35u/108$ [42, 53]. Usually, as already mentioned above, the other contributions are negligible. On the other hand, if the kinetic term is minimal and the potential derivative has a discontinuity, then the third vertex proportional to ϵ_2' is the dominant one. Thus an important new feature of the scenario studied in this paper is that these two vertices are present. Moreover, one can expect the third vertex to be enhanced by the factor $1/c_s^2$ since $c_s \ll 1$. The same mechanism should be valid for the other vertices as well. We are therefore in a rather complicated set-up in which non-Gaussianities are not easy to calculate since all terms contribute and since the mode function has a complicated behaviour. Despite that, it seems clear that the f_{NL} 's parameters will be quite large, especially compared to the Planck constraints: $f_{\text{NL}}^{\text{loc}} = 2.7 \pm 5.8$, $f_{\text{NL}}^{\text{eq}} = -42 \pm 75$ and $f_{\text{NL}}^{\text{ortho}} = -25 \pm 39$ [2]. For instance, using the DBI equation, one obtains $\gamma \lesssim 12$. But, clearly, in our case, the constraint should be much tighter since other terms will contribute. In addition our γ is a time-dependent quantity so the calculation of the contribution of the first term will be modified. To estimate quantitatively the value of f_{NL} is a question that should be addressed by means of numerical calculations, or maybe using the formalism recently developed in [54]. It does not come as a surprise since we have shown before that already the two-point correlation function is an object difficult to calculate. We conclude that non-Gaussianities will be a very important probe to constrain the DBI-Starobinsky model.

To end this paper, let us indicate the main directions for future works. Based on the previous considerations, it seems clear that the most promising direction is the calculation of non-Gaussianities. On the theoretical side, we have a new situation, not envisaged before, in which not only one vertex contributes but many and in a “coupled fashion”, *i.e.* the fact that $c_s \ll 1$ enhancing the contribution coming from the discontinuity of V' . From the observational point of view, given the Planck result, it is clear that the corresponding constraints on the parameters of the model will be very tight. On the other hand, we have seen that the amplitude of the superimposed oscillations can be large (or, at least, seems larger than in the CS-model), even if the parameters are relatively close to standard slow-roll inflation. As a consequence, *a priori*, it remains possible that non-negligible superimposed oscillations improve the fit to the CMB data (especially by matching the Planck anomalies) while, at the same time, equilateral non-Gaussianities remain within the observational bounds. We hope to address this issue in more detail in the near future.

V. ACKNOWLEDGEMENTS

S. Ávila acknowledges financial support from FPI-UAM PhD grants and ‘la Caixa’ postgraduate scholarships. We thank P. Brax and L. Sriramkumar for enlightening discussions.

-
- [1] P. Ade et al. (Planck Collaboration) (2013), 1303.5082.
 - [2] P. Ade et al. (Planck Collaboration) (2013), 1303.5084.
 - [3] J. Martin, C. Ringeval, and V. Vennin (2013), 1303.3787.
 - [4] A. A. Starobinsky, JETP Lett. **55**, 489 (1992).
 - [5] A. A. Starobinsky, Grav.Cosmol. **4**, 88 (1998), astro-ph/9811360.
 - [6] J. Martin and L. Sriramkumar, JCAP **1201**, 008 (2012), 1109.5838.
 - [7] F. Arroja and M. Sasaki, JCAP **1208**, 012 (2012), 1204.6489.
 - [8] D. K. Hazra, L. Sriramkumar, and J. Martin (2012), 1201.0926.
 - [9] M. Alishahiha, E. Silverstein, and D. Tong, Phys.Rev. **D70**, 123505 (2004), hep-th/0404084.
 - [10] E. Silverstein and D. Tong, Phys.Rev. **D70**, 103505 (2004), hep-th/0310221.
 - [11] L. Lorenz, J. Martin, and C. Ringeval, JCAP **0804**, 001 (2008), 0709.3758.
 - [12] L. Lorenz, J. Martin, and C. Ringeval, Phys.Rev. **D78**, 063543 (2008), 0807.2414.
 - [13] J. Martin, C. Ringeval, and V. Vennin (2013), 1303.2120.
 - [14] D. Langlois, S. Renaux-Petel, D. A. Steer, and T. Tanaka, Phys.Rev. **D78**, 063523 (2008), 0806.0336.
 - [15] L. Kofman, A. D. Linde, X. Liu, A. Maloney, L. McAllister, et al., JHEP **0405**, 030 (2004), hep-th/0403001.
 - [16] P. Brax and E. Cluzel, JCAP **1104**, 014 (2011), 1102.1917.
 - [17] P. Brax and E. Cluzel, JCAP **1003**, 016 (2010), 0912.0806.
 - [18] J. Martin and C. Ringeval, JCAP **0608**, 009 (2006), astro-ph/0605367.
 - [19] J. Martin and C. Ringeval, Phys.Rev. **D69**, 083515 (2004), astro-ph/0310382.
 - [20] J. Martin and C. Ringeval, Phys.Rev. **D69**, 127303 (2004), astro-ph/0402609.
 - [21] J. Martin and C. Ringeval, JCAP **0501**, 007 (2005), hep-ph/0405249.
 - [22] E. Komatsu et al. (WMAP Collaboration), Astrophys.J.Suppl. **192**, 18 (2011), 1001.4538.
 - [23] J. Martin and R. H. Brandenberger, Phys.Rev. **D63**, 123501 (2001), hep-th/0005209.
 - [24] X. Chen, R. Easther, and E. A. Lim, JCAP **0804**, 010 (2008), 0801.3295.
 - [25] R. Flauger, L. McAllister, E. Pajer, A. Westphal, and G. Xu, JCAP **1006**, 009 (2010), 0907.2916.

- [26] X. Chen, JCAP **1012**, 003 (2010), 1008.2485.
- [27] L. Leblond and E. Pajer, JCAP **1101**, 035 (2011), 1010.4565.
- [28] M. Aich, D. K. Hazra, L. Sriramkumar, and T. Souradeep (2011), 1106.2798.
- [29] J. Martin, C. Ringeval, and R. Trotta, Phys.Rev. **D83**, 063524 (2011), 1009.4157.
- [30] C. Ringeval, Lect.Notes Phys. **738**, 243 (2008), astro-ph/0703486.
- [31] D. K. Hazra, M. Aich, R. K. Jain, L. Sriramkumar, and T. Souradeep, JCAP **1010**, 008 (2010), 1005.2175.
- [32] R. K. Jain, P. Chingangbam, J.-O. Gong, L. Sriramkumar, and T. Souradeep, JCAP **0901**, 009 (2009), 0809.3915.
- [33] J. Choe, J.-O. Gong, and E. D. Stewart, JCAP **0407**, 012 (2004), hep-ph/0405155.
- [34] C. Dvorkin and W. Hu, Phys.Rev. **D82**, 043513 (2010), 1007.0215.
- [35] M. Park and L. Sorbo, Phys.Rev. **D85**, 083520 (2012), 1201.2903.
- [36] W. Hu, Phys.Rev. **D84**, 027303 (2011), 1104.4500.
- [37] V. Miranda, W. Hu, and P. Adshead, Phys.Rev. **D86**, 063529 (2012), 1207.2186.
- [38] R. Bean, X. Chen, G. Hailu, S.-H. H. Tye, and J. Xu, JCAP **0803**, 026 (2008), 0802.0491.
- [39] D. J. Schwarz, C. A. Terrero-Escalante, and A. A. Garcia, Phys.Lett. **B517**, 243 (2001), astro-ph/0106020.
- [40] S. M. Leach, A. R. Liddle, J. Martin, and D. J. Schwarz, Phys.Rev. **D66**, 023515 (2002), astro-ph/0202094.
- [41] D. J. Schwarz and C. A. Terrero-Escalante, JCAP **0408**, 003 (2004), hep-ph/0403129.
- [42] X. Chen, M.-x. Huang, S. Kachru, and G. Shiu, JCAP **0701**, 002 (2007), hep-th/0605045.
- [43] L. Lorenz, J. Martin, and C. Ringeval, Phys.Rev. **D78**, 083513 (2008), 0807.3037.
- [44] A. Lewis, A. Challinor, and A. Lasenby, Astrophys.J. **538**, 473 (2000), astro-ph/9911177.
- [45] A. Lewis and S. Bridle, Phys.Rev. **D66**, 103511 (2002), astro-ph/0205436.
- [46] A. Gangui, F. Lucchin, S. Matarrese, and S. Mollerach, Astrophys.J. **430**, 447 (1994), astro-ph/9312033.
- [47] A. Gangui, Phys.Rev. **D50**, 3684 (1994), astro-ph/9406014.
- [48] L.-M. Wang and M. Kamionkowski, Phys.Rev. **D61**, 063504 (2000), astro-ph/9907431.
- [49] A. Gangui and J. Martin, Mon.Not.Roy.Astron.Soc. (1999), astro-ph/9908009.
- [50] A. Gangui and J. Martin, Phys.Rev. **D62**, 103004 (2000), astro-ph/0001361.
- [51] A. Gangui, J. Martin, and M. Sakellariadou, Phys.Rev. **D66**, 083502 (2002), astro-ph/0205202.
- [52] J. M. Maldacena, JHEP **0305**, 013 (2003), astro-ph/0210603.
- [53] D. Seery and J. E. Lidsey, JCAP **0506**, 003 (2005), astro-ph/0503692.
- [54] P. Adshead, W. Hu, and V. Miranda (2013), 1303.7004.